

New Extremely Metal-Poor Stars in the Galactic Halo¹

Judith G. Cohen², Norbert Christlieb⁴, Andrew McWilliam³, Stephen Shectman³, Ian Thompson³, Jorge Melendez⁵, Lutz Wisotzki⁶ & Dieter Reimers⁷

ABSTRACT

We present a detailed abundance analysis based on high resolution and high signal-to-noise spectra of eight extremely metal poor (EMP) stars with $[\text{Fe}/\text{H}] \lesssim -3.5$ dex, four of which are new. Only stars with $4900 < T_{\text{eff}} < 5650$ K are included.

Two stars of the eight are outliers in each of several abundance ratios. The most metal poor star in this sample, HE1424–0241, has $[\text{Fe}/\text{H}] \sim -4$ dex and is thus among the most metal poor stars known in the Galaxy. It has highly anomalous abundance ratios unlike those of any other known EMP giant, with very low Si, Ca and Ti relative to Fe, and enhanced Mn and Co, again relative to Fe. Only (low) upper limits for C and N can be derived from the non-detection of the CH and NH molecular bands. HE0132–2429, another sample star, has excesses of N and Sc with respect to Fe.

The strong outliers in abundance ratios among the Fe-peak elements in these C-normal stars, not found at somewhat higher metallicities ($[\text{Fe}/\text{H}] \sim -3$ dex),

¹Based in part on observations obtained at the W.M. Keck Observatory, which is operated jointly by the California Institute of Technology, the University of California, and the National Aeronautics and Space Administration.

²Palomar Observatory, Mail Stop 105-24, California Institute of Technology, Pasadena, Ca., 91125, jlc@astro.caltech.edu, aswenson@caltech.edu

³Carnegie Observatories of Washington, 813 Santa Barbara Street, Pasadena, Ca. 91101, andy, ian, shec@ociw.edu

⁴Current address: Department of Astronomy and Space Physics, Uppsala University, Box 515, 75120 Uppsala, Sweden, formerly at Hamburger Sternwarte, Universität Hamburg, Gojenbergsweg 112, D-21029 Hamburg, Germany, norbert@astro.uu.se

⁵Palomar Observatory, Mail Stop 105-24, California Institute of Technology, Pasadena, Ca., 91125, Current address: Australian National University, Australia, jorge@mso.anu.edu.au

⁶Astrophysical Institute Potsdam, An der Sternwarte 16, D-14482 Potsdam, Germany, lwisotzki@aip.de

⁷Hamburger Sternwarte, Universität Hamburg, Gojenbergsweg 112, D-21029 Hamburg, Germany, dreimers@hs.uni-hamburg.de

are definitely real. They suggest that at such low metallicities we are beginning to see the anticipated and long sought stochastic effects of individual supernova events contributing to the Fe-peak material within a single star. With spectra reaching well into the near-UV we are able to probe the behavior of copper abundances in such extreme EMP stars.

A detailed comparison of the results of the analysis procedures adopted by our 0Z project compared to those of the First Stars VLT Large Project finds a systematic difference for $[\text{Fe}/\text{H}]$ of ~ 0.3 dex, our values always being higher.

Subject headings: nuclear reactions, nucleosynthesis, abundances — stars: abundances — supernovae: general

1. Introduction

Extremely metal poor stars provide important clues to the chemical history of our Galaxy, the role and type of early SN, the mode of star formation in the proto-Milky Way, and the formation of the Galactic halo. The number of extremely metal poor (EMP) stars known is summarized by Beers & Christlieb (2005). They compiled a list of the key properties of the 12 stars identified up to that time with $[\text{Fe}/\text{H}] \lesssim -3.5$ dex¹, 7 of which are EMP giants and subgiants within the range of T_{eff} considered here.

Our 0Z project has the goal of increasing the sample of such stars through data mining of the Hamburg/ESO Survey (HES) (Wisotzki *et al.* 2000). This is an objective prism survey from which it is possible to efficiently select QSOs (Wisotzki *et al.* 2000) as well as a variety of interesting stellar objects, among them extremely metal poor (EMP) stars (Christlieb 2003).

The 0Z project has been systematically searching the database of the HES for this purpose over the past five years. We present in §2 a sample of new EMP giants with $T_{\text{eff}} < 6000$ K and $[\text{Fe}/\text{H}] \lesssim -3.5$ dex which substantially increases the number of such stars known. Details of the analysis are described in §5, while the radial velocity data are discussed in §5.1. The abundance ratios for ~ 20 elements in each of the sample EMP giants are described in §6. In the following section (§7) we check the consistency of the analyses and procedures adopted by our 0Z project with those of the First Stars VLT Large Project using

¹The standard nomenclature is adopted; the abundance of element X is given by $\epsilon(X) = N(X)/N(\text{H})$ on a scale where $N(\text{H}) = 10^{12}$ H atoms. Then $[\text{X}/\text{H}] = \log_{10}[N(\text{X})/N(\text{H})] - \log_{10}[N(\text{X})/N(\text{H})]_{\odot}$, and similarly for $[\text{X}/\text{Fe}]$.

UVES (Cayrel *et al.* 2004) and offer some comments on the implication of our results on the frequency of carbon-enhanced stars. The penultimate section presents a discussion of the implications of our results for early SN and for nucleosynthesis in the forming Galactic halo. A summary of the key results follows. Two appendices which discuss details of a comparison of our work with other large spectroscopic and photometric surveys of EMP stars complete this paper.

2. Sample of Stars

In pursuit of our goal of exploiting the HES to identify new EMP stars, we began with a list of candidates selected from the HES database over the 50% of its area on the sky to which we have access. Our OZ project has now taken moderate resolution spectra of more than 600 candidates with the Double Spectrograph (Oke & Gunn 1982) on the Hale 5-m telescope at Palomar Mountain, and more than 1100 at the 6.5m Clay and Baade Telescopes at the Las Campanas Observatory. These spectra have been processed with the algorithm of Beers *et al.* (1999), which uses a measure of the strength of $H\delta$ and of the 3933 Å line of Ca II, to determine rough metallicities, denoted $[Fe/H](HES)$. Cohen *et al.* (2005) provides a brief description of the vetting process, see also Beers & Christlieb (2005). Those stars of special interest with follow-up spectra from Palomar, including all those with $[Fe/H](HES) < -2.9$ dex, have been observed with HIRES (Vogt *et al.* 1994) at the Keck I telescope over the past four years; a total of ~ 90 such stars have been observed with HIRES to date. In this paper we present analyses of those stars from the Palomar sample with $T_{\text{eff}} < 6000$ K which turned out to be genuine EMP stars with $[Fe/H] \lesssim -3.5$ dex as determined from our high-resolution, high SNR spectra, and which have not already been published in our earlier papers. A future paper will deal with the most extreme metal-poor stars found in the Las Campanas sample. The limitation on T_{eff} ensures that internal comparisons of abundance ratios within the sample will be as reliable as possible.

Five new EMP stars are presented here. One turned out to be a rediscovery of a HK Survey star. This was not realized for a long time due to the 32" difference in the coordinates of CS22949–037 from its discovery by the HK Survey (Beers, Preston & Smetman 1985, 1992), and those of HE2323–0256, found in the HES. It appears that the HK Survey coordinates are sometimes in error by such a large amount, as the updated coordinates for this star given by Cayrel *et al.* (2004) are within 1.5" of those from the HES of HE2323–0256.

We also include a new analysis based on better spectra of the only genuine EMP giant described previously in our published papers, HE0132–2429, part of the Keck Pilot Project (Cohen *et al.* 2002; Carretta *et al.* 2002). We do not consider here the three

EMP dwarfs whose analyses we have published, BS16545–0089 and HE1346–0427 from Cohen *et al.* (2004), nor HE0218–2738, a double lined spectroscopic binary (Cohen *et al.* 2002; Carretta *et al.* 2002). There are many fewer absorption lines detected in these hotter stars and we wish to restrict ourselves to a narrow range in T_{eff} to ensure accurate comparisons within our sample.

We add to our sample the only star from the Hamburg/ESO r-process enhanced star survey (HERES) (Barklem *et al.* 2005; Christlieb *et al.* 2004b) which they believed to have $[\text{Fe}/\text{H}] < -3.5$ dex, HE1300+0157. We also add the star BS16467–062, which is included in the VLT/UVES First Stars program (Cayrel *et al.* 2004). A detailed analysis for the latter, found in the HK Survey, was presented by Francois *et al.* (2003), which was superseded by that of Cayrel *et al.* (2004). Since BS16467–062 and HE2323–0256 are part of the First Stars sample, several analyses have been published for each of these stars. In the present work they serve as comparison objects to determine the consistency of the absolute iron abundance and relative abundances of various elements as deduced by our group versus those of the First Stars VLT large program.

The sample stars are listed in Table 1, which gives their J2000 coordinates, new optical photometry, when available, and other relevant data.

3. Stellar Parameters

We use the procedures described in Cohen *et al.* (2002) and used in all subsequent work by our 0Z project published to date. Our T_{eff} determinations are based on broad band colors $V - I$, $V - J$ and $V - K$. The IR photometry is taken from 2MASS (Skrutskie *et al.* 2006; Cutri *et al.* 2003). We have obtained new photometry at V and I for almost all of the stars discussed here. We use ANDICAM images taken for this purpose over the past two years via a service observing queue on the 1.3m telescope at CTIO operated by the SMARTS consortium. ANDICAM is a dual channel camera constructed by the Ohio State University instrument group². Our ANDICAM program requires photometric conditions, and additional standard star fields, charged to our ANDICAM allocation through NOAO, are always taken for us. Appendix A compares our photometry with that of Beers *et al.* (2007) and with that of the Sloan Digital Sky Survey (York *et al.* 2000).

We derive surface gravities through combining these T_{eff} with an appropriate 12 Gyr isochrone from the grid of Yi *et al.* (2002).

²See <http://www.astronomy.ohio-state.edu/ANDICAM> and <http://www.astro.yale.edu/smarts>.

The resulting stellar parameters, which have been derived with no reference to the spectra themselves, are given in Table 1. The random uncertainties in T_{eff} from photometric errors (see Appendix A) are 100 K. This ignores systematic errors which may be present. The adopted uncertainties in $\log(g)$ are, following the discussion in Cohen *et al.* (2002), $100 d[\log(g)]/dT_{\text{eff}}$ evaluated along the RGB for stars in this extremely low metallicity range, 0.2 dex at $T_{\text{eff}} = 5000$ K and 0.15 dex at 5500 K.

4. Observations

The EMP stars in our sample were observed with HIRES at Keck during various runs over the past 4 years. Details of the best available spectra for each of the new stars are listed in Table 2. Six of these stars were observed with high SNR spectra from HIRES at the Keck Observatory after the recent detector upgrade, which provides complete spectral coverage from 3180 to 5990 Å in a single exposure. Two (HE1356–0622 and HE1347–1025³) have only relatively short exposures with the new detector, used primarily to measure the strength of the NaD lines. Their only high SNR spectra were taken before the upgrade and hence have spectral coverage restricted to 3840 to 5330 Å with no gaps between orders for $\lambda < 5000$ Å, and only small gaps thereafter. The slit width (either 0.86 arcsec, corresponding to a spectral resolution of 46,000, or 1.1 arcsec, which corresponds to a spectral resolution of 35,000) used for each spectrum is indicated in this table as well. Each exposure was broken up into 1200 sec segments to expedite removal of cosmic rays. The goal was to achieve a SNR of 100 per spectral resolution element in the continuum at 4500 Å; a few spectra have slightly lower SNR. This SNR calculation utilizes only Poisson statistics, ignoring issues of cosmic ray removal, night sky subtraction, flattening, etc. The observations were carried out with the slit length aligned to the parallactic angle.

The processing of the spectra was done with MAKEE⁴ and Figaro (Shortridge 1993) scripts, and follows closely that described by Cohen *et al.* (2006). The equivalent widths were measured as described in Cohen *et al.* (2004). Table 4 lists the atomic parameters adopted for each line and their equivalent widths measured in the spectra of each of the 8 EMP stars.

³We are grateful to W. Sargent for obtaining this spectrum.

⁴MAKEE was developed by T.A. Barlow specifically for reduction of Keck HIRES data. It is freely available on the world wide web at the Keck Observatory home page, http://www2.keck.hawaii.edu/inst/hires/data_reduction.html.

5. Analysis

The analysis is identical to that of Cohen *et al.* (2004) with several important additions. In particular we use the model stellar atmosphere grid of Kurucz (1993) and a current version of the LTE spectral synthesis program MOOG (Snedden 1973), which treats scattering as LTE absorption. The improved HIRES spectra now reach into the near-UV, making the NH and redder part of the OH bands accessible. We use the molecular line list of Kurucz (1994), augmented with the strongest atomic features, to analyze the NH band. We use the line list of Gillis *et al.* (2001) for OH. Our nominal Solar CNO abundances are 8.59, 7.93, and 8.83 dex respectively. These are close to those of Grevesse & Sauval (1998), but somewhat larger than the values obtained using 3D model atmospheres by Asplund *et al.* (2004) and Asplund *et al.* (2005). We prefer not to attempt 3D corrections until a full grid of model 3D atmospheres or of corrections to CNO abundances derived from the molecular bands from 3D to 1D models becomes available. For CH and for NH we have adjusted the scale of our gf values so as to reproduce the Solar spectrum, taken from Wallace, Hinkle & Livingston (1998). We adopt dissociation potentials of 3.47 and 4.39 eV (Huber & Herzberg 1979) for CH and OH respectively. For NH we adopt 3.40 eV based on the theoretical calculations of Bauschlicher & Langhoff (1987) and the laboratory spectroscopy of Ervin & Armentrout (1987). Our analysis assumes classical plane parallel stellar atmospheres and LTE, both for atomic and for molecular features.

In view of the inclusion of the near-UV in many of these spectra, a few UV lines of key atomic species have been added to the master line list. These include, for example, three Fe II lines near 3270 Å which are stronger than any in the optical band. This is important as often only the two strongest Fe II lines in the optical are detected in even high quality spectra of such extremely metal poor giants; the remaining optical Fe II lines are too weak. For the most extreme EMP dwarfs, none of the optical Fe II lines can be detected. Inclusion of the UV lines strengthens the determination of the ionization equilibrium between Fe I, with its multitude of detected lines, and Fe II. Lines of species with no detectable optical features, such as V II and Mn II, have also been added. The resonance lines of Cu I near 3250 Å were added as well, as the usual Cu I lines seen in stars with $[\text{Fe}/\text{H}] \sim -2.5$ dex, including those at 5105 and 5782 Å, become undetectable at the extremely low metallicities of the stars studied here. In such cases, the gf values were adopted from Version 3.1.0 of the NIST Atomic Spectra Database (physics.nist.gov/PhysRefData/ASD/index.html). The HFS patterns for the UV Mn II lines are given by Holt, Scholl & Rosner (1999), but these lines in the sample stars are mostly so weak that the corrections are negligible. Those for the UV Cu I lines were downloaded from R. Kurucz’s web site; his primary source was Biehl (1976). The isotope ratio $^{63}\text{Cu}/^{65}\text{Cu}$ was assumed to be the solar value.

Where possible, we have checked the consistency of the scale of the transition probabilities for a given species between the rarely used UV lines and the commonly used optical ones by comparing the derived abundances of lines for the same species as a function of wavelength for a small number of stars with HIRES spectra taken as part of our 0Z project with somewhat higher [Fe/H], including as HD 122563, with weak or no detected CH or NH. The results of this check were satisfactory for Fe II. However, even with HFS included, $\log[\epsilon(\text{Mn})]$ deduced from the 4030 Å triplet of Mn I (the strongest lines in the optical region, two lines of which are sufficiently unblended to use in an abundance analysis) appear to be ~ 0.3 dex lower than those found from the redder optical lines and from the UV resonance lines of Mn II. In the solar spectrum, as well as for HD 122563, the nominal Solar Mn abundance of Anders & Grevesse (1989) is recovered only for lines with $4783 \leq \lambda \leq 6022$ Å, as well as from the Mn II UV lines. A similar problem with the 4030 Å Mn I triplet was noted by Cayrel *et al.* (2004). Bihain *et al.* (2004) has carried out such a consistency check for Cu I. They compare their [Cu/Fe] determinations based on the near-UV resonance lines with those of Mishenina *et al.* (2002) derived from the weak optical lines. They find good agreement, i.e. a mean difference for 16 stars of -0.04 ± 0.04 dex.

Following Cohen *et al.* (2004), we adopt a non-LTE correction for Al I, for which we only detect the resonance doublet at 3950 Å, of +0.60 dex based on the work of Baumüller & Gehren (1996) and Baumüller & Gehren (1997). We adopt a non-LTE correction for Na I, for which we can only observe the two D lines, of -0.20 dex based on the calculations of Takeda *et al.* (2003). No other non-LTE corrections have been applied.

Our abundances for the CNO elements are based on molecular bands of CH, NH and OH respectively. We use 1D model atmospheres to synthesize the molecular features, ignoring any 3D effects, although Collet, Asplund & Trampedach (2006) suggest that these may be very large. They claim that CNO abundances may be overestimated by ~ 0.8 dex as compared to a 1D analysis when molecular bands are used in EMP stars.

Table 5 gives the slope of a linear fit to the abundances determined from the set of Fe I lines as a function of χ (the excitation potential of the lower level), W_λ , and λ , which are most sensitive to T_{eff} , v_t , and the wavelength dependence of any missing major source of continuous opacity, respectively. There are ~ 40 to 60 Fe I lines detected in each star, with χ ranging from 0 to 3 eV. The correlation coefficients $cc(\lambda)$ of the fits with λ are, for all except one of the stars, between 0.11 and -0.20 , indicating that these fits are not statistically significant. The $cc(W_\lambda/\lambda)$ for the fit with W_λ are within the same range for most of the stars. The slopes with χ appear at first sight to be statistically significant with $|cc(\chi)| > 0.4$ for one of the 8 stars; the $cc(\chi)$ are predominantly negative. They reach as low as ~ -0.09 dex/eV for two of the stars. If these slopes were valid, they would

suggest that for these two stars, T_{eff} needs to be decreased by ~ 300 K to achieve excitation equilibrium for Fe I. However, a careful scrutiny of the behavior of the derived Fe abundance from individual Fe I lines indicates that the problem lies largely in the 0 eV lines; for those of higher excitation (the majority of the lines), the deduced abundance shows no statistically significant dependence on χ . A typical example of this is shown in Fig. 1.

Our plots of abundance versus reduced equivalent width indicate that the Fe I overabundances for lines with $\chi < 0.2$ eV do not appear to arise from an inappropriate choice of microturbulent velocity parameters. The effect could be due to systematic errors for gf values of low excitation lines, or may result from resonance scattering (e.g. see Asplund 2005). In resonance scattering the source function, S_ν , is reduced to below the local Planck function, thus leading to a stronger line in non-LTE. Resonance scattering is seen in the Na D lines of metal-poor stars (e.g. Andrievsky *et al.* 2007), the OI triplet at 7774 Å in the Sun and may have affected the abundances from the Ca I 4226 Å resonance line of McWilliam *et al.* (1995a). If resonance scattering is the cause of the small abundance enhancement seen in the 0 eV Fe I lines, the effect should be more pronounced in the weakest low excitation lines; thus a plot of W_λ versus abundance enhancement should show a positive correlation. Proof that resonance scattering is the cause of the apparent overabundances requires a non-LTE abundance calculation for Fe in our stars, which is beyond the scope of this paper.

5.1. Radial Velocities

The radial velocities were determined using the procedure described in Cohen *et al.* (2004), updated to improve the long term stability of v_r measurements; they are given in Table 2. Each individual measured v_r from the spectrum of a star taken with the upgraded HIRES detector for the SNR typical of the present set of spectra taken on a given run now has an internal uncertainty of < 0.2 km s $^{-1}$, with possible long term systematic drifts of comparable size; this was not true of the v_r published in earlier papers of the 0Z project.

For six of our sample EMP stars we have HIRES spectra taken between 2 and 5 years apart. The older spectra have been re-reduced using our improved procedures and codes to measure more accurate v_r . R. Cayrel has generously provided the v_r measured by the First Stars project from their UVES spectra for the two stars discussed here which are in common.

Table 3 compiles the available high precision radial velocities for these EMP stars from HIRES and from UVES. Two of the stars with v_r measurements from multiple HIRES spectra show v_r variations, HE0132–2429 at more than 10σ and HE1012–1540 at the 4σ level. In addition, BS16467–062 may also be a v_r variable, with a difference exceeding 5σ between the

two UVES measurements from M. Spite & R. Cayrel and that from our HIRES spectrum, but this should be verified. Such v_r variations presumably result from orbital motion in a binary system.

6. Abundances

Tables 6 and 7 give the derived abundances for each detected species in each of the 8 EMP giants. We divide the stars into two groups: low C stars with the G band of CH barely detectable, if present at all, and three stars which appear to have C enhanced. The first group includes five of the 8 stars, HE0132–2429, HE1347–1025, HE1356–0622, HE1424–0241 and BS16467–062. The second group includes three stars, two of which (HE1300+0157 and HE2323–0256) are in the present analyses hovering just at the border line of being C-rich, defined by Beers & Christlieb (2005) as $[C/Fe] > +1.0$ dex. The third star, HE1012–1540, is a highly C-enhanced EMP star. The fraction of C-rich stars in our sample of EMP giants with this definition is a minimum of 1/8 and a maximum of 3/8, depending on which side of the boundary of $[C/Fe] = +1.0$ dex the two borderline stars fall.

6.1. The Low Carbon Stars

We first consider the 5 stars with low C. These stars span a relatively small total range in T_{eff} of 420 K, from 4950 to 5370 K. Their spectra show very weak metallic absorption lines and lack strong molecular features, so measuring W_λ for them is straightforward; the uncertainties in the W_λ are thus low, particularly for the three stars with high SNR spectra taken with the updated HIRES detector. A breakdown of the abundance errors resulting from uncertainties in T_{eff} , $\log(g)$, and v_t can be found in Table 6 of Ramírez & Cohen (2003). Given our uncertainties in the determination of the stellar parameters, the dominant contribution to the uncertainties in the abundance ratios $[X/Fe]$ is that of T_{eff} . The contribution from errors in v_t , W_λ and the assumed metallicity of the model atmosphere are small for most elements due to the use of mostly weak lines and to the stars being so metal poor. (Exceptions are Ca I, Mg I and Ni I, where the expected contributions to the uncertainty in $[X/Fe]$ from T_{eff} and from $\log(g)$ are each ≤ 0.05 dex, and Sc II, La II, Ba II and Eu II, where they are each ≤ 0.08 dex in absolute value.) We therefore expect the abundance ratios when compared among this group of stars to have small errors, ± 0.15 dex. Systematic errors of comparable size may exist for the CNO elements as these are derived from hydride bands and accurate values for many molecular parameters are required for their analysis. This estimate is too conservative, at least for comparisons internal to the 0Z project, for neutral species with at

least three detected absorption lines which have a temperature dependence similar to that of Fe I, an example of which is Cr I, when enough lines are detected in a star.

The abundance ratios in these stars among the heavy elements are shown in Fig. 2 for 9 species in the range Ca to Cu. The median is indicated, and stars with $[X/Fe]$ which deviate from the median by more than 0.3 dex are shown individually; these are always either HE0132–2429 or HE1424–0241. If there is an outlier for a particular species, the individual values of $[X/Fe]$ for the remaining four stars in the sample are shown as well. Thus this figure demonstrates graphically how deviant the outliers really are.

The medians show (see Fig. 2) a small excesses for Ca and for Ti with respect to Fe. Cr, Mn and Cu are deficient relative to Fe, while Co is strongly enhanced relative to Fe. Ni appears to be tied to Fe so that $[Ni/Fe] \sim 0.0$ dex. These are in agreement with the usual trend seen among extreme EMP stars as found in our previous work (Cohen *et al.* 2004) and in the First Stars project (Cayrel *et al.* 2004).

The surprise is the outliers. Five species with outliers are marked in Fig. 2, all of which arise in only two stars, HE0132–2429 and HE1424–0241. Spectral regions illustrating lines of three of these cases, contrasting the outlier star with a star close to the median value of $[X/Fe]$, are shown in Figs. 3, 4 and 5. The stars displayed in each figure have been chosen to have T_{eff} as close to each other as possible. These figures demonstrate the reality of the outlier in $[X/Fe]$ for each of Sc II, Ti II and Mn I. The spectra of the each outlier star for each of these five cases have been checked twice. Two independent HIRES spectra exist for several of these stars. There is no question that the outliers in each of [Ca, Sc, Ti, Mn, Co/Fe] are real.

Fig. 6 shows the behavior of $[X/Fe]$ for 7 light elements in the range C to Ca for the five C-normal stars. Upper limits are ignored, and only one of these stars has a detectable NH band. Again there are outliers. One might expect outliers among those elements (C, N, O, Na, Mg, and Al) where mixing of proton-burning material has already been demonstrated to occur among luminous EMP giants by Spite *et al.* (2005) and Spite *et al.* (2006), while Andrievsky *et al.* (2007) present slight modifications in the details due to non-LTE effects without altering the overall picture. Large variations in $[N/Fe]$ are clearly present among this small sample of C-normal EMP giants, as illustrated in Fig. 7, where it is shown that HE0132–2429 has a strong enhancement for $[N/Fe]$.

The most peculiar star in this sample of EMP giants, HE1424–0241, is also the most metal poor, with $[Fe/H] \sim -4$ dex. The very low $[Si/Fe]$ and other abundance anomalies found in a preliminary analysis of this star were briefly reported in Cohen *et al.* (2007). HE1424–0241 has a ratio of $[Si/Fe]$ which is 1.2 dex below that of any other star in the

present sample, a result which is completely unexpected. Fig. 8 shows the spectral region of the 3905 Å Si I line to demonstrate the obvious reality of this very discrepant abundance ratio. This star also has anomalously low [Ca/Fe] and moderately low [Ti/Fe], accompanied by unusually high [Mn/Fe] (by 0.6 dex) and [Co/Fe]. The G band of CH and the NH band at 3360 Å are not detected in the HIRES spectra of this star, implying fairly low upper limits for C and for N.

The EMP giant HE0132–2429 has [Sc/Fe] higher than any other star in the sample of C-normal stars by 0.4 dex, accompanied by very high [N/Fe], and [N/C] > 0. HE1356–0622 shows an apparent small excess for [Na/Fe] and for [Si/Fe]. The modest anomalies in this star are small enough that their reality is dubious.

The plots comparing spectral regions around key absorption lines presented here reinforce our claim that most if not all of the discrepant points in Figs. 2 and 6 are unquestionably real, and not the result of observational error nor of uncertainties in the analysis. They are not consistent with a dependence on condensation temperature nor on first ionization potential. Table 6 presents a summary of the abundance ratios found among the five C-normal stars.

We have presented in Tables 6 and 7 the first Cu abundances for extreme EMP stars, made possible by the high efficiency of HIRES in the near-UV, so that we can reach Cu I resonance lines near 3250 Å. Fig. 9 displays [Cu/Fe] as a function of [Fe/H] for our sample of EMP giants (including one whose analysis has not yet been published). Earlier results using the weak optical Cu I lines by Mishenina *et al.* (2002) (for the giants in their sample) and by Simmerer *et al.* (2003) who compiled the means for Galactic globular clusters are shown in this figure. A steady decrease of [Cu/Fe] as the Fe-metallicity decreases was found in previous work. Our new results demonstrate that [Cu/Fe] reaches a plateau at low Fe-metallicity below [Fe/H] –2.0 dex which continues through the extreme EMP stars, as might be expected if Cu is formed primarily in massive stars.

The behavior of the heavy element ratio [Sr/Ba] is presented in Fig. 10. Here the values from all the stars in our sample of candidate EMP giants from the HES from our published and unpublished work are indicated as well to provide guidance as to the typical behavior. Stars from the present sample often have very weak lines of both of these elements. If no detected line has $W_\lambda < 10 \text{ mÅ}$, we consider the abundance $\epsilon(\text{Sr})$ or $\epsilon(\text{Ba})$ for that star to be an upper limit.

The abundance ratio $\epsilon(\text{Sr})/\epsilon(\text{Ba})$ ranges over more than a factor of 100, in agreement with McWilliam *et al.* (1995b) and McWilliam (1998). The fractions predicted to arise from pure *r* or *s* process nucleosynthesis for the Sun, taken from Simmerer *et al.* (2004), are

indicated in Fig. 10 by the dashed and solid horizontal lines. CS22892–052, the prototype for the rare extreme r -process stars, shows $[\text{Sr}/\text{Ba}] -0.4$ dex (see, e.g. Sneden *et al.* 2003), a value somewhat below the r -process line indicated in Fig. 10.

The presence of numerous EMP stars with $[\text{Sr}/\text{Ba}]$ larger than that from either the standard s or r -process demonstrates that another process must exist which produces the light neutron capture elements, and in particular Sr, in EMP stars, without producing those in the second peak (i.e. Ba), as was originally suggested by McWilliam *et al.* (1995b). Early calculations by Prantzos, Hashimoto & Nomoto (1990) have been updated and augmented by Travaglio *et al.* (2004), who emphasize the many nucleosynthetic processes that can produce Sr, Y and Zr, and who suggest again that a secondary source of Sr from an as yet unidentified nucleosynthetic site is required.

Supernova calculations by Woosley & Hoffman (1992) found production of elements significantly heavier than the iron-peak, up to $A \sim 100$, occurs for high neutron excess material (greater than $\eta \sim 0.05$) during the alpha-rich freezeout. They also suggested that the alpha-rich freezeout might merge, naturally, into an r -process.

Chieffi & Limongi (2004) computed supernova yields for a range of masses and metallicities, including charged particle reactions up to Mo. In their models they found that elements heavier Zn could only be produced for metallicities greater than $Z/Z_{\odot} = 10^{-3}$, essentially confirming the neutron-excess sensitivity found by Woosley & Hoffman (1992) for the production of elements up to $A \sim 100$. This metallicity limit excluded the supernovae considered by Chieffi & Limongi (2004) as sources for the enhancements of elements up to $A \sim 100$ seen in EMP stars (e.g. as found by McWilliam 1998).

Nomoto *et al.* (2006) explored theoretical supernova and hypernova yields; while they included the alpha-rich freezeout in their calculations, they only considered species up to $A=74$. Their hypernovae were characterized with kinetic energies more than 10 times that of normal core-collapse supernovae. It was found that in the complete Si-burning region of hypernovae elements produced by the alpha-rich freezeout are enhanced. Thus, we speculate that some form of alpha-rich freezeout, perhaps from hypernova explosions, with metallicities lower than the low limit determined by Chieffi & Limongi (2004), may yet provide an explanation for the extra source of $A \sim 100$ elements seen in some EMP stars (also known as a “second r -process”).

Most of the stars with $[\text{Sr}/\text{Ba}]$ significantly less than that of the r -process (and of the s -process as well) are carbon stars with highly enhanced Ba from the s -process running at low Fe-metallicity (see, e.g. Busso, Gallino & Wasserburg 1999). Some of the EMP stars studied here fall somewhat below the r -process line, but not by more than 2σ .

All of the EMP stars in the present sample, including the three C-rich stars, have $[\text{Ba}/\text{Fe}] < -0.2$ dex. With such weak lined stars, and no excess of Ba in any of them, no other heavy elements beyond the Fe-peak besides Ba and Sr could be detected in any of the 8 EMP stars studied here.

6.2. The Stars with Higher C

There are three stars with the G band of CH obviously much stronger than the five C-normal stars discussed above. Two of the then have larger enhancements of C than of N, but one (HE2323–0256, CS22949–037) has $[\text{N}/\text{Fe}] > [\text{C}/\text{Fe}]$, as shown in Fig. 11. In two of the three stars, including the highly N-enhanced star, Na and Mg are also enhanced, while the enhancement of Al is more modest. Such enhancements have been seen among other very metal poor carbon stars, for example HE0336+0113 from our 0Z survey, with $[\text{Mg}/\text{Fe}] +1.0$ dex (Cohen *et al.* 2005), the EMP giant CS29498–043, studied by Aoki *et al.* (2004) with highly enhanced Na and Mg as well, and the very extreme EMP dwarf CS22958–042 (T_{eff} 6250 K, $[\text{Fe}/\text{H}] -2.85$ dex) with $[\text{Na}/\text{Fe}] +2.8$ dex analyzed by Sivarani *et al.* (2006). On the other hand, HE1300+0157, which has the smallest C+N-enhancement of the three stars, $[\text{C}/\text{Fe}] \sim 1.2$ dex, has only an upper limit for N (from NH), with highly enhanced O (from OH). It shows normal abundances for all other detected elements.

Each of the three C-rich EMP stars shows good agreement for the abundance ratios $[\text{X}/\text{Fe}]$ for the elements with detected features from Ca through Cu with each other and with the median from the five C-normal stars. This is illustrated in Fig. 12. The C-enhancement, even when extreme, does not affect the relative abundances of elements in this range, which includes the Fe-peak, as was suggested earlier by, e.g. Cohen *et al.* (2006).

7. Comparison with the Abundance Analyses of Cayrel *et al.* (2004)

The 0Z project and the First Stars project of Cayrel *et al.* (2004) using UVES at the VLT are two large independent efforts to determine the chemical abundance ratios in EMP stars and use those to draw inferences on the properties of the early Galaxy, the first supernovae, etc. Our sample largely consists of new EMP stars we have found through painstaking, time consuming searches of the HES database coupled with the expenditure of very large and generous allocations of telescope time. We have observed a few stars from thee sample of the First Stars Survey at the VLT (Cayrel *et al.* 2004) and have analyzed them independently. We compare our results with those of (Cayrel *et al.* 2004) to determine the consistency of

the absolute iron abundance and relative abundances of various elements as deduced by our group versus those of the First Stars VLT large program.

We begin by testing the measured equivalent widths for the two stars in common, HE2323–0256 (a.k.a. CS22949–037) and BS16467–062, the latter of which we added to our sample specifically for this purpose. There are 79 lines in common for BS16467–062, with a mean difference in W_λ of 1.8 mÅ and σ of the differences of 4.4 mÅ. This extremely good agreement is shown in Fig. 13. The agreement in measured W_λ for HE2323–0256 (a.k.a. CS22949–037) is not quite as good (see Fig. 14); the dispersion of the differences in measured W_λ for the 66 lines in common is 9.5 mÅ, with a mean difference of only 0.3 mÅ. Most of the dispersion arises from 5 discrepant lines, as is shown in Fig. 14. M. Spite advises (private communication, June 2007), on behalf of the First Stars Project, that their published W_λ for these 5 lines are not correct, and that the correct values from their UVES spectra are much closer to those given here in Table 4. She further advises that she believes that their problems with W_λ are restricted to this particular star.

We next examine the scale of the transition probabilities adopted by each group. For 43 Fe I lines in common in the spectrum of BS16467–062, the mean difference in $\log(gf)$ is only 0.004 dex, with σ for the differences of 0.06 dex. The scale of the gf values for all lines of species in common with Cayrel *et al.* (2004) have been compared. The maximum scale difference for the lines of a given species was only 0.04 dex (occurring for Fe II), with the largest dispersion about the mean for the lines in common reaching 0.07 dex (for Ti II). Thus we find that the parameters adopted for atomic lines by the two groups are in very good agreement, and specifically for Fe I are identical in the mean to within ± 0.01 dex.

We have adopted the Schlegel, Finkbeiner & Davis (1998) reddening map, which has a small but non-zero reddening at the Galactic pole, while the First Stars project appears to be using the older Burstein & Heiles (1982) values based on 21 cm HI surveys. This map has zero reddening at the Galactic pole. Hence we have systematically larger reddening values for each star than does the First Stars project.

A detailed discussion of the differences in the stellar parameters between us and the First Stars project and the differences in abundance, both absolute (i.e. [Fe/H]) and ratios with respect to Fe ([X/Fe]), is given in Appendix B. Overall for a particular star with measured W_λ for a set of detected absorption features and values of observed optical and 2MASS colors, the [Fe/H] value derived by the First Stars project as described in Cayrel *et al.* (2004) will be systematically ~ 0.3 dex lower than that for the same star as analyzed by the 0Z project. It is interesting to note that the sample of stars analyzed by Aoki *et al.* (2005) also included two stars in common with the First Stars project sample. Aoki *et al.* (2005) derived [Fe/H] values higher than those of Cayrel *et al.* (2004) by ~ 0.2 dex.

Table 1 of Cohen *et al.* (2007) compares the mean for $[X/Fe]$ for C-normal EMP giants between our 0Z survey and the First Stars survey of Cayrel *et al.* (2004). A detailed comparison for a small number of individual stars in common is given in Appendix B. We find much better agreement of the abundance ratios $[X/Fe]$ between the two large surveys than for absolute Fe-metallicities $[Fe/H]$. This is as expected since many of the error terms in the absolute iron abundance $[Fe/H]$ largely cancel out in an abundance ratio $[X/Fe]$. If we ignore C deduced from an analysis of the CH band and N inferred from the UV NH band, we find differences in $[X/Fe]$ for 11 or 12 elements in a star ranging from -0.07 to $+0.05$ dex when we adopt their equivalent widths but use our stellar parameters. Somewhat larger differences, ± 0.15 dex with $\sigma = 0.10$ dex, occur when we analyze our own HIRES spectra with our own choice of stellar parameters, in part because of the errors in the W_λ of Cayrel *et al.* (2004). As indicated above, only a maximum of ± 0.04 dex of these differences arise from differences in the scale of the transition probabilities adopted by each of these large surveys.

7.1. Comparison with the HERES Sample

Analyses of 253 stars from the Hamburg/ESO *r*-process enhanced star survey (HERES, Christlieb *et al.* 2004b) was presented by Barklem *et al.* (2005). This survey relied on modest SNR high resolution spectra of candidate EMP giants from the HES. We have observed with HIRES at the Keck I telescope the most Fe-poor star found in that survey, HE1300+0157, as a comparison object. A very detailed abundance analysis based on a high quality Subaru/HDS spectrum for this star was recently presented by Frebel *et al.* (2007).

Both HERES and Frebel *et al.* (2007) utilize the relations between broad band colors and T_{eff} for giants of Alonso, Arribas & Martinez-Roger (1999) evaluated at $[Fe/H] -2.0$ dex, as these relations have not been calibrated adequately at still lower metallicities. As was discussed in Cohen *et al.* (2002), while the MARCS and ATLAS9 T_{eff} color-relations are in very good agreement, they disagree with those of Alonso, Arribas & Martinez-Roger (1999). In this regime of T_{eff} , $\log(g)$ and $[Fe/H]$, the difference in deduced T_{eff} for a fixed $V - K$ color is ~ 200 K, with the value derived from the Alonso, Arribas & Martinez-Roger (1999) relations being cooler. The T_{eff} adopted by Barklem *et al.* (2005), Frebel *et al.* (2007), and that we derive for HE1300+0157 are 5411, 5450, and 5630 K respectively. This difference in T_{eff} corresponds to a difference in $[Fe/H]$ of ~ 0.35 dex, with HE1300+0157 having the higher Fe-metallicity of -3.4 dex in our analysis instead of the value they obtained, -3.7 dex.

We first consider the comparison for the star HE1300+0157 if we adopt T_{eff} and $\log(g)$ from Barklem *et al.* (2005), but analyze with our own codes and atomic parameters our own set of W_λ from our HIRES/Keck spectra. Overall, with this assumption, the agree-

ment between the results presented here based on high SNR Keck/HIRES spectra and those of HERES is very good given the lower SNR of their spectra and the automatic analysis codes employed in the analysis of Barklem *et al.* (2005). For the 10 elements in common, the agreement in $\log\epsilon(X)$ is in all cases within the errors assigned by HERES for absolute abundances (their “errA” values, ranging from ~ 0.2 to 0.3 dex), and in almost all cases is within the smaller relative errors they assigned for star-to-star comparison within HERES. The techniques employed by HERES are certainly more than adequate to find interesting EMP stars and determine the general nature of their chemical inventory.

We detected several additional elements beyond those that HERES could reach. We suggest, as did Frebel *et al.* (2007), that the HERES claimed detection of Y using their automatic abundance analysis code is almost surely incorrect; they found $[Y/Fe] +0.56$ dex. They could not detect Sr; we find a marginal detection of a single Sr II line which yields $[Sr/Fe] = -1.55$ dex. Given this very low Sr abundance, any accessible optical Y line would be expected to be undetectable.

We now compare our derived $[Fe/H]$ and abundance ratios $[X/Fe]$ for HE1300+0157 with those of the very detailed and careful analysis by Frebel *et al.* (2007). Their T_{eff} is 180 K cooler than ours, hence they derive $[Fe/H]$ 0.34 dex lower than we do. However, the difference in abundance ratios should be smaller assuming the same stellar parameters are adopted.

For the CNO elements, we note that there is agreement to within 0.2 dex for the $[C/Fe]$ and $[O/Fe]$ abundance ratios in this star between our analysis and that of Frebel *et al.* (2007), while both fail to detect the NH band and only have an upper for $[N/Fe]$. Our $[C/Fe]$ is identical to that derived by Lucatello *et al.* (2006), who analyzed the HERES spectra for the CNO elements. Since their $[Fe/H]$ for this star was only -2.9 dex, this implies a difference in $\epsilon(C)$ between the value they derive and that of either of the two high dispersion analyses of about a factor of 3 (0.5 dex), with the value of Lucatello *et al.* (2006) for HE1300+0157 being too large.

We have carried out the comparison for this star adopting first the stellar parameters of Frebel *et al.* (2007), then those we have derived. In both cases we use our own set of W_λ measured from our HIRES spectra. The results are given in Table 10. Our measured W_λ for Fe I lines show no systematic difference with those of Frebel *et al.* (2007). Similarly $\Delta(Fe) = [Fe\text{ I}/H] - [Fe\text{ II}/H]$ has the same sign (positive) in both analyses, but our ionization equilibrium is slightly better than theirs ($\Delta(Fe) = 0.08$ vs 0.15 dex) for the identical stellar parameters. However, $\log\epsilon(Fe\text{ I})$ is slightly higher in our analysis (by 0.13 dex) with same stellar parameters; the origin of this offset is not clear.

Adopting their (cooler) T_{eff} , we find that of the 17 elements in common (ignoring upper limits), $\log[\epsilon(X)]$ differs by less than 0.10 dex for 7 of them, but disagrees by more than 0.15 dex for 6 species. Adopting our hotter T_{eff} raises $[\text{Fe}/\text{H}]$ substantially. But the values of $[\text{X}/\text{H}]$ are only slightly altered, $|\Delta[\text{X}/\text{H}]| < 0.15$ dex for most elements in our analysis. The largest change in abundance ratio is seen for C, which is derived from the CH molecular band; with the higher T_{eff} $[\text{C}/\text{Fe}]$ increases by ~ 0.2 dex. The same holds for O (from the OH band).

8. Discussion

Our 0Z survey and the First Stars survey at the VLT (see, e.g. Cohen *et al.* 2004, Cayrel *et al.* 2004), following in the footsteps of many earlier studies, including, for example, McWilliam *et al.* (1995a) and McWilliam *et al.* (1995b), have established over the past five years the general behavior of abundances among EMP stars, with substantial samples of stars analyzed with $[\text{Fe}/\text{H}] < -2.5$ dex. If one ignores the light elements which might be affected by proton burning, definite trends of $[\text{X}/\text{Fe}]$ with $[\text{Fe}/\text{H}]$ have been established beginning with Ca and extending through the Fe-peak which hold down to $[\text{Fe}/\text{H}] \sim -4$ dex. The data available to date show that there is a scatter about these trends which for most stars with normal carbon abundances and for most elements is not larger than the observational uncertainties. A substantial theoretical effort has gone into calculations of nucleosynthesis yields in core collapse SN directed towards understanding the behavior of these “typical” VMP and EMP stars. The work of Chieffi & Limongi (2004), Kobayashi *et al.* (2006) and Tominaga, Umeda & Nomoto (2007) are examples of recent computations for grids of metal-poor stars over a range of initial mass and chemical composition. These models have been tuned to reproduce the previously observed trends of abundance ratios among “typical” EMP stars.

In comparing the properties of our sample of EMP giants with the predictions of such calculations, it behooves us to recall the enormous difficulty of these calculations and the many parameters whose values must be calculated from theory, assumed, or inferred from the data and which substantially affect the resulting predicted nucleosynthesis yields. Among the most crucial of these factors are the explosion energy, the mass cut, the neutron excess, and previous mass loss in earlier evolutionary stages.

There are three stars in the present sample of EMP giants which we consider as “typical”. They have normal or low carbon. Their abundance ratios follow the patterns previously delineated by our work and that of the First Stars project. However, there are also two C-normal stars which are definite outliers. Some abundance ratios in these two stars are

definitely anomalous. The small T_{eff} range of our sample discussed here ensures that inter-comparisons within the 0Z project set of abundance analyses are valid and that differences exceeding 0.3 dex are real. Furthermore, in Table 1 of Cohen *et al.* (2007) we compared our mean abundance ratios with those of Cayrel *et al.* (2004) for those “typical” giants studied by each group. In our case this included our published and unpublished abundance analyses, and for the First Stars project we relied upon the fits tabulated in Cayrel *et al.* (2004). The agreement was very good, within 0.10 dex, with one exception (Mg). Although we emphasize again that we have shown here that our $[\text{Fe}/\text{H}]$ scale is systematically 0.3 dex higher than that of Cayrel *et al.* (2004), the consequences for abundance ratios of differences in the details of the analyses between these two surveys are much smaller. We are therefore confident that any outliers found are real and are not the result of problems or uncertainties in our measurements or analyses.

HE1424–0241, with $[\text{Fe}/\text{H}] \sim -4$ dex, is the most extreme outlier we have found. Its peculiarities were briefly described in Cohen *et al.* (2007). This extreme EMP giant has a very low abundance of Si, and moderately low Ca and Ti, with respect to Fe. Si, Ca and Ti are produced primarily via explosive α -burning. But Mg/Fe, where Mg is produced largely by hydrostatic α -burning, is normal in this star. Mn and Co are enhanced with respect to Fe. Only (low) upper limits for C and for N could be determined. Older calculations of nucleosynthetic yields by Woosley & Weaver (1995) come close to reproducing at least some of this behavior with ejecta from SN biased towards the lower end of the relevant mass range, but more current grids of SNII nucleosynthesis fail to reproduce the very unusual chemical inventory seen in this extreme EMP star. We defer to our theoretical colleagues to try to find an explanation for this very peculiar star.

The anomalies seen in HE1424–0241 are unique and, as far as we are aware, are not seen in any other EMP giant studied to date. This is illustrated in Fig. 16 and 17, which show $[\text{Si}/\text{Fe}]$ and $[\text{Ca}/\text{Fe}]$ as a function of $[\text{Fe}/\text{H}]$ for all the C-normal giants analyzed by our 0Z project to date, all those of the First Stars project (Cayrel *et al.* 2004), and those from several other sources noted in the figure legends. In both cases, HE1424–0241 has the lowest value by far of the relevant abundance ratio.

There is one star, CS22966–043, studied by Preston & Sneden (2000) and again by Ivans *et al.* (2003) which has abundance ratios somewhat similar to those of HE1424–0241. CS22966–043 has $[\text{Fe}/\text{H}] -1.9$ dex, with $[\text{Si}/\text{Fe}] -1.0$ dex (Ivans *et al.* 2003) and $[\text{Ca}/\text{Fe}] -0.2$ dex, with $[\text{Cr}/\text{Fe}]$ and $[\text{Mn}/\text{Fe}]$ somewhat high and $[\text{Sr}/\text{Fe}]$ somewhat low for its Fe-metallicity. CS22966–043, however, has $T_{\text{eff}} = 7200$ K. It is a SX Phe variable and a binary. It shows rotation, with $v_{\text{rot}} \sin(i) = 20 \text{ km s}^{-1}$ (Preston 1996), not uncommon among stars in the Preston & Sneden (2000) sample of blue metal poor stars. It may be a blue straggler, the

outcome today of extensive past mass transfer within the binary system. Ivans *et al.* (2003) attribute its anomalies to local differences in the chemical history within different regions of the Galactic halo, presumably arising from accretion of one or more dwarf satellite galaxies. We assume, perhaps incorrectly, that whatever may be causing its anomalies is not directly relevant to those of the EMP giant HE1424–0241.

The second of the two outliers is HE0132–2429, with $[\text{Fe}/\text{H}] = -3.55$ dex. The spectrum of this star indicates moderately high $[\text{C}/\text{Fe}]$, very high $[\text{N}/\text{Fe}]$, and high $[\text{Sc}/\text{Fe}]$. We suggest that this is the result of a major contribution to its chemical inventory from a SNII with a higher than typical mass. Limongi & Chieffi (2006) reproduce the general nature of these anomalies with a massive SNII with $M \sim 60M_{\odot}$ (see their Fig. 5). Although this calculation was carried out for solar metallicity, we take it as applying at least partially to extremely metal poor SNII. We could not locate any published SNII models with nucleosynthetic yields for a large set of isotopes for such massive extremely metal poor stars; the published grids typically end at $40M_{\odot}$, with some studies, for example Umeda & Nomoto (2002), then jumping to treat very massive pair instability SN with $M \sim 150M_{\odot}$, omitting the mass range of “normal” SNII with $M > 50M_{\odot}$. The very recent calculations of Tominaga, Umeda & Nomoto (2007) for nucleosynthesis in Pop III SNII explosions end at $50M_{\odot}$.

The peculiarities in abundance ratios found in HE0132–2429 are reminiscent of those found in the most Fe-poor star known, HE1327–2326 (Frebel *et al.* 2005), which also has N highly enhanced (with C enhanced as well, but not by as much) and high Sr relative to Fe. The Sc II lines are too weak to be detected in such an extreme star even if the same anomaly were present for this element as well.

HE1356–0622 is a modest outlier in $[\text{Na}/\text{Fe}]$ and in $[\text{Si}/\text{Fe}]$, being high in both cases by perhaps ~ 0.5 dex. However, $[\text{Na}/\text{Fe}]$ shows a definite range among EMP giants (Cayrel *et al.* 2004), which Spite *et al.* (2006) subsequently explained as mixing of material processed through proton-burning along the RGB, thus enhancing Na by ~ 0.5 dex (see also Andrievsky *et al.* 2007, for a discussion of non-LTE effects.). Since HE1356–0622 is one of the coolest stars in our sample of EMP giants, it presumably is among those with the highest luminosity and thus has a high probability of being a mixed star. The apparent anomaly in $[\text{Si}/\text{Fe}]$ is due primarily to the extremely large deficiency of that ratio in HE1424–0241, which couples with our adopted definition of “anomalous” via a median over our small sample of C-normal EMP giants. After careful consideration, we find that HE1356–0622 is probably a mixed EMP giant and has no statistically significant anomalies in its abundance ratios for the set of elements we have detected.

The three more C-rich stars in the present sample of EMP giants all obey patterns

previously seen for such stars (see, e.g. Cohen *et al.* 2005 or Aoki *et al.* 2006). Two of them show strong enhancements of the light elements up to and including Al; one does not.

There are two stars in our sample of EMP giants with $[N/C] > 0$, one of which is very highly N-enhanced. CS 22949-037 (a.k.a HE2323–0256), is a N-rich star, with $[N/Fe] +2.16$ dex, while $[C/Fe]$ is $+0.97$ dex. HE0132–2429 is a milder case of a star with $[N/C] > 0$. Several similar stars are known, although EMP C-rich stars with $[N/C] < 0$ are much more common than EMP giants with $[N/C] > 0$. If we assume that the C-rich EMP giants are the result of mass transfer across a binary system when the former primary was an AGB star, then predictions of nucleosynthesis in AGB stars (Lattanzio 1992, Herwig 2004, and references therein) suggest that hot bottom burning in intermediate mass AGB stars (3 to $6 M_{\odot}$) leads to strong N-enhancements

Johnson *et al.* (2006) discuss the predicted frequency of N-enhanced stars with $[N/C] > 0$ as a function of mass of the AGB star contributing. They suggest that N-rich stars represent the contribution from the upper mass limit of such stars near $\sim 6 M_{\odot}$, and note that their observed frequency appears to be quite low compared to that expected for a normal mass distribution of AGB stars. They speculate that factors which decrease the efficiency of mass transfer in binary systems with large mass ratios may be responsible for the apparent lack of N-enhanced stars.

To summarize the situation as we view it, HE1424–0241 and HE0132–2429, both analyzed here, are the only EMP giants known to us which show peculiar abundance ratios among the Fe-peak elements. One EMP dwarf, HE2344–2800 with $[Fe/H] \sim -2.7$ dex, first studied in the Keck Pilot Project, was a suspected outlier, with $[Cr/Fe] \sim 0.3$ dex higher than typical EMP dwarfs, a large sample of which were studied in Cohen *et al.* (2004). Analysis of a new HIRES spectrum of this EMP dwarf taken in Oct. 2004 confirms the excess in $[Cr/Fe]$, and suggests an excess in $[Mn/Fe]$ of ~ 0.5 dex as well. Many EMP stars show unexpectedly high CNO abundances, which are likely due to intrinsic production followed by mixing (for luminous giants only) or pollution from a former AGB binary companion. A smaller number of stars, including two of the three C-rich stars studied here, show large enhancements of the light elements Na, Mg and Al as well. All such α -enhanced stars with the exception of BS16964–002, very recently discovered by Aoki *et al.* (2007), are C-rich; Aoki’s new star is, however, highly O-rich. A few stars, such as CS22952–015 (McWilliam *et al.* 1995a) and CS22169–035 (Cayrel *et al.* 2004) show small (at least compared to those of the present sample) deficiencies of the α -elements, with normal C.

With better spectra and analyses, and the larger sample of known EMP stars enabled in part by our searching for such in the Hamburg/ESO Survey, we are now able to discern the impact on the chemical inventory of a star from contributions by individual SNII among

extreme EMP stars. At slightly higher Fe-metallicity, we see abundance ratios which show slow trends as functions of $[\text{Fe}/\text{H}]$ with low dispersions about the mean trends which presumably arise from summing the ejecta of SNII over a stellar population with a normal (i.e. Salpeter or similar) initial mass function. These trends can often be reproduced in detail by theoretical models of Galactic chemical evolution containing the most recent nucleosynthetic yields such as those of Prantzos (2006) or Matteucci (2007). It is now up to the theorists who model SNII explosions to try to develop a set of nucleosynthesis yields which will lead to the variety of chemical inventories we have seen in the EMP stellar population in the Milky Way, particularly among the lowest $[\text{Fe}/\text{H}]$ stars known in the Galaxy, and especially for the very anomalous extreme EMP star HE1424–0241.

Turning to the elements beyond the Fe-peak, another by now well established observational fact is the decoupling between the production of the Fe-peak elements and the heavy neutron capture elements. The ratios of $[\text{Sr}/\text{Fe}]$ and $[\text{Ba}/\text{Fe}]$ among the EMP stars analyzed by our OZ project, including those discussed here, show a very wide range among both the C-normal and C-rich EMP stars (see Fig. 10). It is interesting to note that no star in the present sample, neither C-normal nor C-rich, has $[\text{Ba}/\text{Fe}] > -0.2$ dex. Among more metal-rich C-rich stars, the fraction of stars with enhancements of the *s*-process elements is large, exceeding 75% (see, e.g. Cohen *et al.* 2006).

8.1. Implications for C/Fe ratio and Frequency of C-enhanced stars

The fraction of C-enhanced stars among EMP stars is a very contentious issue. Adopting the definition of C-enhanced stars of Beers & Christlieb (2005) as those with $[\text{C}/\text{Fe}] > 1.0$ dex, recent values for this fraction from several independent survey for stars with $[\text{Fe}/\text{H}] < -2.0$ dex cover the range from $> 21 \pm 0.2\%$ (Lucatello *et al.* 2006) to $9 \pm 2\%$ (Frebel *et al.* 2007), with our OZ survey yielding a preliminary value of $14 \pm 4\%$ (Cohen *et al.* 2005).

The samples are in each case reasonably large, but there is a fairly large range in the deduced frequency of C-rich EMP stars. This suggests that differences in the analysis are contributing to this problem. It is not surprising in the context of the previous discussion (see, for example, that of §7.1) that the fraction of C-rich stars calculated from a set of different independent analyses of large samples would result in different estimates from different surveys. Our $[\text{Fe}/\text{H}]$ values are systematically higher than those of Cayrel *et al.* (2004) by ~ 0.3 dex, and the differences in C and N abundances determined from molecular bands between the two surveys show a larger dispersion than do the abundances based on atomic absorption lines. Stars near the boundary of the C-enhanced class could easily be shifted into or out of the C-rich class as a result of small systematic differences between the various

ongoing large projects. This would affect such frequency calculations, whatever the specific abundance characteristic of interest might be.

Since there are many stars near the boundary of the C-enhanced class as defined above, we suggest that a substantial part of the variation in the deduced fraction of C-enhanced EMP stars arises from such differences in the details of the analysis. It is thus extremely important for people engaged in this type of work to publish the full details of their analyses, as we did in Cohen *et al.* (2006), and to analyze a few stars in common with other major groups working in this area. Among the details that must be described, in addition to those discussed above, is the issue of the way one handles the recent upheaval in the Solar CNO abundances through the work of Asplund *et al.* (2004) and Asplund *et al.* (2005) with 3D models.

The modified definition of the cutoff for enhanced $[C/Fe]$ suggested by Aoki *et al.* (2007) offers the advantage of a cleaner cut with fewer stars near the boundary between C-normal and C-enhanced classes. It is preferable to the definition we are using, which is that of Beers & Christlieb (2005). With the latter definition, two of the three stars are just at the boundary, while with the newer definition, all three of the C-rich stars discussed here would clearly be considered C-rich.

9. Summary

We have presented detailed abundance analyses of five extremely metal poor giants which are newly discovered from our datamining of the Hamburg/ESO Survey. One of these turned out to be a rediscovery of a star found in the HK Survey with an unusually large error in its published coordinates. We include here a new analysis based on better spectra of HE0132–2429, part of the Keck Pilot Project (see Cohen *et al.* 2002 and Carretta *et al.* 2002). We also analyze new high resolution and high signal-to-noise ratio spectra of the only EMP giant found in the HERES project (Barklem *et al.* 2005) and of an EMP giant from the First Stars project to use as a calibration object for comparison of the two projects, for a total sample of 8 EMP giants.

The high quality of our HIRES spectra and our discovery of many more EMP stars, including some close to -4 dex, makes it possible to search for, to find, and to confirm outliers which have anomalous abundance ratios $[X/Fe]$ among the Fe-peak elements, where such have not been detected previously. The lowest metallicity star in our sample, HE1424–0241, with $[Fe/H] -3.95$ dex, has only upper limits for the C and N abundances, based on our non-detection of the G band of CH and of the 3360 Å band of NH. This star shows highly

anomalous abundance ratios, with extremely low $[\text{Si}/\text{Fe}]$ (< -1 dex) and very low $[\text{Ca}/\text{Fe}]$ (-0.6 dex) and $[\text{Ti}/\text{Fe}]$ (-0.18 dex), while $[\text{Mg}/\text{Fe}]$ is normal. Mg is produced in hydrostatic α -burning, while the other three elements are made in explosive α -burning. In essentially all other EMP stars, these three abundance ratios are positive. These deficits in HE1424–0241 are accompanied by strong excesses for the odd atomic number elements, so that $[\text{Mn}/\text{Fe}]$ and $[\text{Co}/\text{Fe}]$ are significantly larger than is typical of all other EMP giants. We speculate that the parcel of gas from which this star formed in the early Milky Way contained ejecta from only a few SNII, and was deficient in ejecta from core collapse SN whose progenitors had masses at the upper end of the relevant range. The nucleosynthesis was such that the explosive α -elements (Si, Ca and Ti) were not produced by the SNII at typical rates, while the hydrostatic α -element Mg, formed during the course of normal stellar evolution even in zero metallicity stars, was produced at normal rates.

A second outlier, HE0132–2429, shows enhanced Sc relative to Fe, with $[\text{N}/\text{C}] > 0$. We suggest that this chemical inventory of this star had the opposite bias, namely a larger contribution from SNII toward the upper end of the progenitor mass range near $60M_{\odot}$. The remaining three C-normal stars have abundance ratios typical of slightly more metal rich EMP stars; they do not show any detectable anomalies in their chemical inventory.

No other EMP giant known to us shows peculiar abundance ratios among the Fe-peak elements. One EMP dwarf, HE2344–2800, first studied in the Keck Pilot Project, and now revisited with a better HIRES spectrum, appears to have $[\text{Cr}/\text{Fe}] \sim 0.3$ dex and $[\text{Mn}/\text{Fe}]$ of ~ 0.5 dex higher than typical EMP dwarfs, a large sample of which were studied in Cohen *et al.* (2004). C and N have only upper limits in this hot dwarf, where the molecular bands are, even for normal $[\text{C}/\text{Fe}]$ ratios, very weak and difficult to detect. Many EMP stars show unexpectedly high CNO abundances, which are likely due to intrinsic production followed by mixing (for luminous giants only) or pollution from a former AGB binary companion. A smaller number of stars, including two of the three C-rich stars studied here, show large enhancements of the light elements Na, Mg and Al as well. All such α -enhanced stars with the exception of BS16964–002, very recently discovered by Aoki *et al.* (2007), are C-rich, and this star is highly O-rich.

The behavior of the C-rich stars contains no surprises. Two in our present sample have large enhancements of the light elements through Al; the third shows normal abundance ratios for Na, Mg and Al with respect to Fe. Two of the sample stars have $[\text{N}/\text{C}] > 0$, which is not common among C-rich EMP giants. It is generally believed that C-rich EMP stars are the result of mass transfer within a binary system when the former primary was an AGB star. If this is true, nucleosynthesis calculations by Lattanzio (1992), Herwig (2004) and references therein suggest that to produce such a large excess of N the former primary must

have a mass towards the upper end of the range for AGB stars.

We present the first determination of $[\text{Cu}/\text{Fe}]$ for EMP giants below $[\text{Fe}/\text{H}] -3$ dex based on the rarely measured UV resonance lines of Cu I near 3250 Å. We find that the plateau level which was suggested for $[\text{Cu}/\text{Fe}]$ for dwarfs with $[\text{Fe}/\text{H}] < -2$ dex by Bihain *et al.* (2004) continues to even lower metallicities.

The heavy neutron capture elements are low in all eight EMP stars in our sample, with $[\text{Ba}/\text{Fe}] < -0.2$ dex. This is rare among more Fe-rich C-stars, which often have strong *s*-process enhancements. The ratio $\epsilon(\text{Ba})/\epsilon(\text{Sr})$ varies by more than a factor of 100 among the stars studied here, and suggests again that another nucleosynthesis mechanism that preferentially produces the light neutron capture elements such as Sr is required.

A careful comparison of the procedures and results of the detailed abundance analyses carried out by our 0Z project with those of the First Stars project (Cayrel *et al.* 2004) demonstrates that there is a systematic offset between the deduced $[\text{Fe}/\text{H}]$ values; ours being on average 0.3 dex higher. Thus the most metal poor star we found, HE1424–0241, with $[\text{Fe}/\text{H}] -3.95$ dex based on our 0Z project analysis, would translate roughly into -4.2 dex if it were analyzed by the First Stars project of Cayrel *et al.* (2004). For elements which display measurable atomic absorption features, the differences between these two projects results in systematic changes in abundance ratios with respect to Fe which are much smaller.

Inter-comparison between surveys of abundances $[\text{X}/\text{Fe}]$ derived from molecular bands, typically used to determine CNO abundances, is much less common and more difficult to carry out. Systematic differences between surveys for CNO abundances from CH, NH, CN, CO or OH bands may be common and may be larger than for elements where atomic lines can be utilized. Any such systematic differences between surveys may affect the deduced fraction of C-rich stars found in a survey and may contribute to the wide range in published values for this parameter.

10. Appendix A: Comparison of Photometry

We have observed ~ 100 EMP candidates with ANDICAM in queue mode over the past three years. We calibrate to the Johnson-Kron-Cousins photometric system using standard star fields from Landolt (1992). The observer at CTIO running the queue only carries out our program if the night is believed to be photometric. Data from nights which at sunset were believed to be photometric, but subsequently the observer changed his opinion of the sky conditions, were discarded. The zero points of our photometric calibration are based on two sets of images of standard star fields per night in almost all cases, and never more than

two. Most stars were observed only on one night; about 1/3 were observed on two nights, and a few on three nights.

We assess whether our assigned photometric errors for ANDICAM photometry of the HES candidate EMP stars are valid by comparison of stars from our sample which are included in much larger, and hopefully better calibrated, photometric surveys. This is a key issue since we use this photometry, together with J, H, K_S from 2MASS, to determine stellar parameters.

We compare our values with those from the SDSS (York *et al.* 2000) DR4 release (Adelman-McCarthy *et al.* 2006), using the transformations of Allyn Smith *et al.* (2002) for Johnson V and Kron-Cousins I . There are 26 stars in common. The mean difference in V and in I between that we measure using ANDICAM and that from the SDSS database appropriately transformed is less than 0.01 mag. The dispersion about the mean is 0.06 mag for each of V and I , somewhat larger than one might expect for our nominal errors of ± 0.03 mag for each combined with the nominal uncertainties of ± 0.02 mag for the SDSS. This suggests that our assessment of the uncertainty in our ANDICAM photometry may be somewhat underestimated.

The SDSS is a very large area survey with a very extensive photometric calibration effort, and our ANDICAM measurements agree well in the mean with the SDSS values, suitably transformed. This suggests that the photometric calibration of our ANDICAM data has no systematic errors.

The recent large photometric survey of EMP candidate stars of Beers *et al.* (2007) includes 17 stars from our ANDICAM sample. Beers *et al.* (2007) include data taken at many sites with many different instruments on many different runs. For these 17 stars, our V is fainter by 0.05 mag on average, with σ of the differences being 0.05 mag. Our $V - I$ colors are identical to within ± 0.01 mag on average with those of Beers *et al.* (2007) for the 12 stars with such colors in the survey of Beers *et al.* (2007), with σ of the difference being 0.03 mag. The (identical) systematic difference in V and in I may arise from calibration difficulties across a survey with such a wide variety of data sources.

HE1424–0241, the most metal-poor star discussed here, has $V(\text{ANDICAM}, \text{SDSS}, \text{Beers}) = 15.47, 15.36, 15.32$ mag respectively, and is among the three stars with the largest deviation in V for both of these comparisons. Its I mag is the same (differing by only 0.015 mag) for the SDSS and for the ANDICAM data, while the Beers *et al.* (2007) photometry for this star has $V - I$ identical to the ANDICAM result, but V brighter by 0.15 mag. If we assume the SDSS V, I to be correct, then we have underestimated T_{eff} for this star by ~ 130 K, the nominal uncertainty we adopt for this key stellar parameter is 100 K.

11. Appendix B: Details of the Comparison with the First Stars Project of Cayrel *et al.* (2004)

In this appendix we provide additional details, beyond the discussion given in §7, of the comparison of the analyses we have carried out for EMP giants with those of the First Stars project as given in Cayrel *et al.* (2004).

We selected a representative sample of stars from Cayrel *et al.* (2004) to cover the range of stellar parameters of interest here ($[\text{Fe}/\text{H}]$ below -3 dex and $\log(g)$ as expected for RGB stars). Three values of T_{eff} determined for each of these stars are shown in Table 11. The first is the value we would derive using the codes and procedures of the OZ project, including reddening from the map of Schlegel, Finkbeiner & Davis (1998). The second is that we would derive if we used $E(B - V)$ from Cayrel *et al.* (2004) instead. The third is that adopted by the First Stars project, taken from Table 4 of Cayrel *et al.* (2004). In all cases, the V mag given in Table 2 of Cayrel *et al.* (2004) was used. T_{eff} for the second and third cases are given in the table as differences from that of our OZ project.

At first sight the differences between the T_{eff} adopted by each project for the representative sample of stars given in the last column of Table 11 are satisfactory considering the quoted accuracies of T_{eff} by us of ± 100 K and by the First Stars project of ± 80 K. However, we stress that this is a systematic, not a random, effect. Table 11 shows, by comparing the first and second values of T_{eff} given for each star, that the somewhat larger values of $E(B - V)$ that we adopt result in our T_{eff} being higher than that of the First Stars project by up to ~ 100 K. This difference depends both on the reddening difference for the particular star (i.e. where the star is in the sky) and on T_{eff} for the star, as hotter stars have smaller values of $\Delta(V - K, V - J)/\Delta(T_{\text{eff}})$.

In addition, for a specified set of stellar colors and a fixed choice of reddening, comparing the second and third choices for T_{eff} , we find that our T_{eff} are higher by up to 100 K. This must arise from some systematic difference in the transformation within the grid of colors (specifically $V - J$ and $V - K$) and the stellar parameters for EMP giants. It should be noted that the T_{eff} given by Cayrel *et al.* (2004) are based on the Alonso, Arribas & Martinez-Roger (1999) relations while ours are based on those of the MARCS and ATLAS model atmosphere grids. This issue was discussed in Cohen *et al.* (2002), where it was demonstrated that the MARCS and ATLAS9 T_{eff} color-relations are in very good agreement, but that they disagree with those of Alonso, Arribas & Martinez-Roger (1999). We also note that the Alonso, Arribas & Martinez-Roger (1999) color relations have not been calibrated adequately at the very low values of $[\text{Fe}/\text{H}]$ considered here; a theoretical calibration is easier to achieve at present than an observational one for EMP stars.

The result of adding these two effects is that our T_{eff} would be from 30 to 165 K hotter than those adopted by Cayrel *et al.* (2004) for the same input set of observed colors, with the hotter stars in the sample ($T_{\text{eff}} \sim 5200$ K) having larger differences than the cooler ones; the coolest stars in our sample have $T_{\text{eff}} \sim 4900$ K. This of course will result in a systematic offset such that the $[\text{Fe}/\text{H}]$ value deduced for a star with a particular set of W_λ will be higher as determined by the 0Z project than as determined by the First Stars project (Cayrel *et al.* 2004). This is accompanied by a smaller effect on the deduced abundance ratios, as we will see below.

Since Cayrel *et al.* (2004) use ionization equilibrium to determine $\log(g)$, given a T_{eff} , while we use evolutionary tracks, there is some scatter of the difference of $\log(g)$ between the two projects for a given star. In most cases the difference is small; the largest difference among the stars compared in Table 11 is 0.4 dex for the same input parameters.

We next isolate the differences introduced into the abundance ratios by the different abundance analysis codes and model atmosphere grids between our 0Z project and the First Stars Project. Recall that we use model atmospheres from ATLAS (Kurucz 1993) while the First Stars project uses OSMARCS models (Gustafsson *et al.* 2002).

We first note that changing to the latest and currently preferred Kurucz models which have a somewhat different treatment of convection with no overshooting described in Castelli, Gratton & Kurucz (1997) and an improved opacity distribution function (which are labeled as “ODFNEW” models) leads to very small changes (not exceeding 0.01 dex) in the derived $\log[\epsilon(\text{X})]$ for all species considered here. The predicted model colors $V - J$ and $V - K$ differ by less than 0.02 mag in this range of $[\text{Fe}/\text{H}]$ and T_{eff} , introducing a change of less than 50 K in deduced T_{eff} . Since these stars are so metal-poor, the details of the treatment of the line opacity used in computing the model atmosphere do not matter.

For this test, we assume, for a given star, the same stellar parameters as Cayrel *et al.* (2004) derived. We then carry out an abundance analysis using our codes and our model atmospheres appropriate to those input stellar parameters, and compare the resulting $[\text{Fe}/\text{H}]$ values and abundance ratios $[\text{X}/\text{Fe}]$. First we compare the deduced values of $\log[\epsilon(\text{X})]$ for three stars. The first case we examined is the bright EMP giant CD $-38\ 245$. We use the W_λ and gf values from Cayrel *et al.* (2004); we do not have any HIRES spectra of this star. For the other two stars, BS16467–062 and CS22949–037 (a.k.a. HE2323–0256) we have independent HIRES spectra; we use our own measured W_λ and our own adopted atomic parameters.

The comparison for the three stars is shown in Fig. 18. This figure shows our absolute abundances being systematically about 0.15 dex larger for all species. This difference is

similar to that found by Luck, Kovtyuk & Andrievsky (2006) (see their Fig. 1), who have carried out a similar test for stellar parameters appropriate to Cepheid variables. This systematic offset would be largely eliminated if we were to use a stellar atmosphere which was ~ 90 K lower than the T_{eff} adopted by the First Stars project. The agreement for the C and N abundances, with differences as large as 0.4 dex, is not as good. This is not surprising, as we have shown in §7 that the gf values for atomic absorptoin lines adopted by both projects are in very good agreement. The C and N abundances, on the other hand, are derived from molecular bands and many more parameters enter, none of which have been compared between the two projects.

The offset from equality shown in Fig. 18 does not affect the deduced abundance ratios $[X/\text{Fe}]$ derived from our work and the First Stars project as the offset is approximately constant for all species considered. However the First Stars project adopts $\log\epsilon(\text{Fe}) = 7.50$ dex for the Sun, while we use a value 0.05 dex smaller. Since, as we have shown earlier, the gf value scales are identical, we will therefore see a systematic difference of 0.05 dex in all values of $[X/\text{Fe}]$ and in $[\text{Fe}/\text{H}]$, with our values being higher (i.e. more metal-rich). This is in addition to the offset of 0.15 dex due to differences in the model atmosphere grids and analysis codes.

For CD–38 245 both analyses give very good ionization equilibrium, so it matters little whether one uses Fe I or Fe II as the reference. Ideally, since $\log\epsilon(\text{FeII})$ is less sensitive to T_{eff} , it would be better to use that in calculating $[\text{Fe}/\text{H}]$ and $[X/\text{Fe}]$, but there are few Fe II lines detected in these EMP stars, and many of those detected are very weak with somewhat unreliable W_λ . The differences in $[X/\text{Fe}]$ for the 12 species in common (ignoring the reference species, Fe I) range from -0.07 to $+0.05$ dex, with a mean of -0.02 dex and σ of 0.04 dex, which we consider very good agreement.

The difference in the deduced abundance ratios between our 0Z project and the First Stars project for HE2323–0256, ignoring N (deduced from the NH band at 3360 \AA in both cases), ranges from -0.18 to $+0.11$ dex for the 11 species in common, with a mean of -0.07 dex and σ 0.10 dex. (That for $[\text{N}/\text{Fe}]$ is 0.38 dex, with our value being lower.) Part of this may arise in the problem with the W_λ for this star; incorrect values were published by Cayrel *et al.* (2004) for at least 7% of the lines in common with our 0Z values given here in Table 4 (M. Spite, private communication, July 2007). The ionization equilibrium of Fe is good in both analyses.

BS 16467–062, the third case we checked, gives similar results. Here, with the stellar parameters set by the First Stars project, the difference in $\log\epsilon(\text{Fe I})$ is 0.16 dex, with our value again being higher. The ionization equilibrium in our solution for this set of stellar parameters is $\log(\epsilon)(\text{Fe I}) - \log(\epsilon)(\text{Fe II}) + 0.04$ dex; for the First Stars project derived

+0.12 dex.

But the true comparison is what happens when we use the stellar parameters derived with our own codes and procedures and the reddening values we adopt (i.e. our systematically higher T_{eff} as compared to those of the First Stars project). For BS 16467–062, if we compare $\log\epsilon(\text{Fe I})$ as published by Cayrel *et al.* (2004) versus that given in Table 6 and 7, the difference in $[\text{Fe}/\text{H}]$ 0.30 dex, with our value being higher. The higher T_{eff} we adopt (164 K higher than that of the First Stars project) based on our higher reddening and on our T_{eff} scale is somewhat compensated by the difference in adopted $\log(g)$. The difference in adopted T_{eff} for CS22949-037 (a.k.a. HE2323–0256) between the two projects is small only because our V mag from ANDICAM photometry is 0.05 mag fainter than that adopted by Cayrel *et al.* (2004). We thus find a difference of +0.18 dex in the final deduced $[\text{Fe}/\text{H}]$, our value being higher. This, given the essentially identical T_{eff} , reflects just the difference in analysis details discussed above.

In summary, it appears that the different analysis codes, and stellar atmospheres grids adopted lead to $[\text{Fe}/\text{H}]$ values from our 0Z project being systematically 0.15 ± 0.03 dex higher than those of the First Stars project. The difference becomes somewhat larger, ~ 0.25 dex, when the hotter stellar parameters determined from the independent codes, procedures, and adopted reddening map of our 0Z project are used instead of those adopted by Cayrel *et al.* (2004). There is an additional contribution of 0.05 dex to the difference in derived $[\text{Fe}/\text{H}]$ from the two projects which arises from the difference in the adopted Solar Fe abundance. Overall, the $[\text{Fe}/\text{H}]$ value derived by the First Stars project as described in Cayrel *et al.* (2004) will be systematically ~ 0.3 dex lower than that for the same star, the same set of W_λ , and the same set of observed stellar photometry as analyzed by the 0Z project.

We are grateful to the many people who have worked to make the Keck Telescope and HIRES a reality and to operate and maintain the Keck Observatory. The authors wish to extend special thanks to those of Hawaiian ancestry on whose sacred mountain we are privileged to be guests. Without their generous hospitality, none of the observations presented herein would have been possible. Some of the data presented herein were obtained at the Palomar Observatory. This publication makes use of data from the Two Micron All-Sky Survey, which is a joint project of the University of Massachusetts and the Infrared Processing and Analysis Center, funded by the National Aeronautics and Space Administration and the National Science Foundation. J.G.C. is grateful to NSF grant AST-0507219 for partial support. N.C. is a Research Fellow of the Royal Swedish Academy of Sciences supported by a grant from the Knut and Alice Wallenberg Foundation. He also acknowledges financial support from Deutsche Forschungsgemeinschaft through grants Ch 214/3 and Re 353/44. We thank W. Huang for help accessing the SDSS database.

REFERENCES

- Adelman-McCarthy, J. K., *et al.*, 2006, ApJS, 162, 38
- Allyn Smith, J. *et al.*, 2002, AJ, 123, 2121
- Alonso, A., Arrivas, S. & Martinez-Roger, C., 1996, A&A, 313, 873
- Alonso, A., Arrivas, S. & Martinez-Roger, C., 1996, A&AS, 140, 261
- Amiot C., 1983, ApJS, 52, 329
- Anders, E. & Grevesse, N., 1989, Geochim. Cosmochim. Acta, 53, 197
- Andrievsky, S. M., Spite, M., Korotin, S. A., Spite, F., Bonifacio, P., Cayrel, R., Hill, V. & Fracois, P., 2007 A&A (in press),
- Aoki, W., Norris, J. E., Ryan, S. G., Beers, T. C., Christlieb, N., Tsangarides, S. & Ando, H., 2004, ApJ, 608, 971
- Aoki, W. *et al.*, 2005, ApJ, 632, 611
- Aoki, W., Beers, T. C., Christlieb, N., Norris, J. E., Ryan, S. G. & Tsangarides, 2007, ApJ, in press
- Asplund, M., Grevesse, N., Sauval, A. J., Allende Prieto, C. & Kisselman, D., 2004, A&A, 417, 751
- Asplund, M. 2005, ARA&A, 43, 481
- Asplund, M., Grevesse, N., Sauval, A. J., Allende Prieto, C. & Blomme, R., 2005, A&A, 431, 693
- Barklem, P. S. *et al.*, 2005, A&A, 439, 129
- Baumüller, D. & Gehren, T., 1996, A&A, 307, 961
- Baumüller, D. & Gehren, T., 1997, A&A, 325, 1088
- Bauschlicher, N. B. & Langhoff, S. R., 1987, Chem. Phys. Lett. 135, 67
- Beers, T.C., Preston, G.W. & Shectman, S., 1985, AJ, 90, 2089
- Beers, T.C., Preston, G.W. & Shectman, S., 1992, AJ, 103, 1987
- Beers, T. C., Rossi, S., Norris, J. E., Ryan, S. & Shefler, T., 1999, AJ, 117, 981

- Beers, T. C. & Christlieb, N., 2005, ARA&A, 43, 531
- Beers, T. C., *et al.*, 2007, ApJS, 168, 128
- Bihain, G., Israelian, G., Bonifacio, P. & Molaro, P., 2004, A&A, 423, 777
- Biehl, D., 1976, Diploma thesis, Kiel University
- Bonifacio, Molaro, Beers, T.C., Vladilo, 1998, A&A, 332, 672
- Burstein, D & Heiles, C., 1982, AJ, 87, 1165
- Busso, M., Gallino, R. & Wasserburg, G.J., 1999, ARA&A, 37, 239
- Carretta, E., Gratton, R. G., Cohen, J. G., Beers, T. C. & Christlieb, N., 2002, AJ, 124, 481
- Castelli, F., Gratton, R. G. & Kurucz, R. L., 1997, A&A, 318, 841
- Cayrel, R. *et al.* 2004, A&A, 416, 1117
- Chieffi, N. & Limongi, M., 2004, ApJ, 608, 405
- Christlieb, N., 2003, Rev. Mod. Astron. 16, 191
- Christlieb, N., Gustafsson, B., Korn, A. J., Barklem, P. S., Beers, T. C., Bessell, M. S., Karlsson, T. & Mizuno-Wiedner, M., 2004, ApJ, 603, 708
- Christlieb, N., *et al.*, 2004, A&A, 428, 1027
- Cohen, J. G., Christlieb, N., Beers, T. C., Gratton, R. G. & Carretta, E., 2002, AJ, 124, 470
- Cohen, J. G., Christlieb, N., McWilliam, A., Sheckman, S., Thompson, I., Wasserburg, G. J., Ivans, I., Dehn, Karlsson, T. & Melendez, J., 2004, ApJ, 612, 1107
- Cohen, J. G. *et al.*, 2005, ApJ, 633, L109
- Cohen, J. G. *et al.*, 2006, AJ, 132, 137
- Cohen, J. G., McWilliam, A., Christlieb, N., Sheckman, S., Thompson, I., Melendez, J., Wisotzki, L. & Reimers, D., 2007, ApJ, 659, L161
- Collet, R., Asplund, M. & Trampedach, R., 2006, ApJ, 644, L121
- Cutri, R. M. *et al.*, 2003, “Explanatory Supplement to the 2MASS All-Sky Data Release, <http://www.ipac.caltech.edu/2mass/releases/allsky/doc/explsup.html>

- Ervin, K. M., & Armentrout, P. B., 1987, J.Chem.Phys., 86, 2659
- Francois et al, 2003, A&A, 403, 1105
- Frebel, A., *et al.*, 2005, Nature, 434, 871
- Frebel, A., *et al.*, 2007, ApJ, 658, 545
- Fulbright, J. P., 2000, AJ, 120, 1841
- Gillis, J. R., Goldman, A, Stark, G & Rinsland, CP, 2001, JQSRT, 68, 225
- Gratton, R. & Sneden, C., 1991, A&A, 241, 501
- Grevesse, N. & Sauval, A. J., 1998, Space Science Reviews, 85, 161
- Gustafsson, B., Edvardsson, B., Eriksson, K., Mizuno-Weidner, M., Jørgensen, U. G. & Plez, B., 2002, in ASP Conf.Ser.288, *Stellar Atmospheres Modeling*, ed. I. Hubeny, D. Mihalic & K. Werner, (San Francisco, ASP), 331
- Herwig, F., 2004, ApJ, 605, 425
- Holt, R.A., Scholl, T.J. & Rosner, S.D., 1999, MNRAS, 306, 107
- Houdashelt, M. L., Bell, R. A. & Sweigart, A. V., 2000, AJ, 119, 1448
- Huber, K. P. & Herzberg, G., 1979, *Constants of Diatomic Molecules*, (New York, Van Nostrand)
- Ivans, I. I., Sneden, C., Renee James, C., Preston, G. W., Fulbright, J. P., Hoflich, P. A., Carney, B. W. & Wheeler, J. C., 2003, ApJ, 592, 906
- Johnson, J., 2002, ApJS, 139, 219
- Johnson, J. A., Herwig, F., Beers, T. C. & Christlieb, N., 2006, ApJ, in press
- Kobayashi, C., Umeda, H., Nomoto, K., Tominaga, N. & Ohkubo, W., 2007, ApJ, 653, 1145
- Kurucz, R. L., 1993, ATLAS9 Stellar Atmosphere Programs and 2 km/s Grid, (Kurucz CD-ROM No. 13)
- Kurucz, R. L., 1994, Diatomic molecular data for opacity calculations, (Kurucz CD-ROM No. 15)
- Landolt, A. U., 1992, AJ, 104, 340

- Lattanzio, J. C., 1992, Pub. Astronomical Soc. of Australia, 10, 120
- Limongi, M. & Chieffi, A., 2006, in *The Multicolored Landscape of Compact Objects and Their Explosive Origins*, to be published by AIP (also available as astro-ph/0611140)
- Lucatello, S., Beers, T., Christlieb, N., Barklem, P., Rossi, S., Marsteller, B., Sivarani, T. & Lee, Y. S., 2006, ApJ, 652, L37
- Luck, R. E., Kovtyuk, V. V. & Andrievsky, S. M., 2006, AJ, 132, 902
- Matteucci, F., 2007, in *Emission Line Universe*, see astro-ph/07040770
- McWilliam, A., Preston, G. W., Sneden, C. & Sheckman, S., 1995, AJ, 109, 2736
- McWilliam, A., Preston, G. W., Sneden, C. & Searle, L., 1995, AJ, 109, 2757
- McWilliam, A., 1998, AJ, 115, 1640
- Mishenina, T. V., Kovtyukh, V. V., Soubiran, C., Travaglio, C. & Busso, M., 2002, A&A, 396, 189
- Nomoto, K., Tominaga, N., Umeda, H., Kobayashi, C., & Maeda, K. 2006, Nuclear Physics, A777, 424 (see also astro-ph/0605725)
- Norris, J. E., Ryan, S. G. & Beers, T.C., 1997, ApJ, 489, L169
- Norris, J. E., Ryan, S. G. & Beers, T.C., 2001, ApJ, 561, 1034
- Oke, J. B. & Gunn, J. E., 1982, PASP, 94, 586
- Plez, B. & Cohen, J. G., 2005, A&A, 434, 1117
- Plez, B., Cohen, J. G. & Melendez, J., 2005, in IAU Symposium 228, *From Lithium to Uranium: Elemental Tracers of Early Stellar Evolution*, ed. V. Hill, P. Francois & F. Primas, Cambridge University Press, pg. 267
- Prantzos, N., Hashimoto, M. & Nomoto, K., 1990, A&A, 234, 211
- Prantzos, N., 2006, in *Nuclei in the Cosmos IX*, CERN, Geneva, July 2006, ed. A. Mengoni et al.
- Preston, G. W., 1996, in *The Formation of the Galactic Halo – Inside and Out*, ed. H. L. Morrison & A. Sarajedini, ASP Conf. Ser. 92
- Preston, G. W. & Sneden, C., 2000, AJ, 120, 1014

- Ramírez, S. V. & Cohen, J. G., 2003, *AJ*, 125, 224
- Schlegel, D. J., Finkbeiner, D. P. & Davis, M., 1998, *ApJ*, 500, 525
- Shortridge K. 1993, in *Astronomical Data Analysis Software and Systems II*, A.S.P. Conf. Ser., Vol 52, eds. R.J. Hannisch, R.J.V. Brissenden, & J. Barnes, 219
- Simmerer, J., Sneden, C., Ivans, I. I., Kraft, R. P., Shetrone, M. A. & Smith, V. v., 2003, *AJ*, 125, 2018
- Simmerer, J., Sneden, C., Cowan, J. J., Collier, J., Woolf, V. M. & Lawler, J. E., 2004, *ApJ*, 617, 1091
- Skrutskie, M. F. *et al.*, 2006, *AJ*, 131, 1163
- Sivarani, T. *et al.*, 2006, *A&A*, 459, 125
- Sneden, C., 1973, Ph.D. thesis, Univ. of Texas
- Sneden, C., *et al.*, 2003, *ApJ*, 591, 936
- Spite, M. *et al.*, 2005, *A&A*, 430, 655
- Spite, M. *et al.*, 2006, *A&A*, 455, 291
- Takeda, Y., Zhao, G., Takada-Hidai, M., Chen, Y. Q., Saito, Y. & Zhang, H. W., 2003, *Chinese Jrl Astron & Astrophys*, 3, 316
- Tominaga, N., Umeda, H. & Nomoto, K., 2007, *ApJ*, 660, 516
- Travaglio, C., Gallino, R., Arnone, E., Cowan, J., Jordan, F. & Sneden, C., 2004, *ApJ*, 601, 864
- Umeda, H. & Nomoto, K., 2002, *ApJ*, 565, 385
- Vogt, S. E. *et al.* 1994, *SPIE*, 2198, 362
- Wallace, L., Hinkle, K. & Livingston, W. C., 1998, “An Atlas of the Spectrum of the Solar Photosphere from 13,500 to 28,000 cm^{-1} ”, N.S.O. Technical Report 98-001, <ftp://nsokp.nso.edu/pub/atlas/visatl>.
- Wisotzki, L., Christlieb, N., Bade, N., Beckmann, V., Köhler, T., Vanelle, C. & Reimers, D., 2000, *A&A*, 358, 77
- Woosley, S. E., & Hoffman, R. D. 1992, *ApJ*, 395, 202

Woosley, S. E. & Weaver, T. A., 1995, ApJS, 101, 181

Yi, S., Demarque, P., Kim, Y.-C. , Lee, Y.-W., Ree, C. Lejeune, Th. & Barnes, S., 2001, ApJS, 136, 417

York, D. *et al.*, 2000, AJ, 120, 1579

Table 1. New EMP Stars With $T_{eff} < 6000$ K From the OZ Project

ID	Coords. (J2000)	V ^a (mag)	I ^a (mag)	E(B–V) ^b (mag)	T_{eff} (K)	$\log(g)$ (dex)	v_t (km s ^{–1})
HE0132–2429 ^f	01 34 58.8 –24 24 18	14.82	...	0.012	5294	2.75	1.8
HE1012–1540	10 14 53.5 –15 55 54	14.04	13.21	0.070	5620	3.40	1.6
HE1347–1025	13 50 22.4 –10 40 19	15.06	14.16	0.058	5195	2.50	1.8
HE1356–0622	13 59 30.3 –06 36 35	14.31	13 36	0.030	4947	1.85	2.2
HE1424–0241	14 26 40.3 –02 54 28	15.47	14.54	0.064	5193	2.50	1.8
HE2323–0256 ^c	23 26 29.8 –02 39 58	14.41	13.40	0.051	4915	1.70	2.0
From Other Surveys:							
HE1300+0157 ^d	13 02 56.3 +01 41 51	14.11	13.39	0.022	5632	3.37	1.3
BS16467–062 ^e	13 42 00.6 +17 48 48	14.09 ^e	...	0.018	5364	2.95	1.6

^aOur photometry from ANDICAM images.

^bBased on the reddening map of Schlegel, Finkbeiner & Davis (1998).

^cRediscovery of CS22949–037 from the HK Survey.

^dFrom HERES (Christlieb *et al.* 2004b; Barklem *et al.* 2005).

^eStar from the HK Survey included in the First Stars (Cayrel *et al.* 2004) sample, V mag from this source.

^fStar from the Keck Pilot Project, V from Cohen *et al.* (2002).

Table 2. Details of the HIRES Observations

ID	Exp.Time (sec)	Julian Date (–2453000.00)	SNR ^a	Slit Width (")	v_r ^b (km s ^{–1})
HE0132–2429	7200	289.89	95	0.86	+289.2
HE1012–1540	3600	489.77	109	0.86	+226.2
HE1300+0157	3600	843.87	>110	1.1	+73.4
HE1347–1025	3600	149.80	80	1.1	+48.6
HE1356–0622	3600	149.89	105	1.1	+93.5
HE1424–0241	6000	844.96	90	1.1	+60.4
HE2323–0256	7200	312.76	100	0.86	–125.9
BS16467–062	3600	490.02	100	0.86	–91.7

^aSNR per spectral resolution element in the continuum at 4500 Å.

^bHeliocentric v_r .

Table 3. Radial Velocities for Stars with Multiple High Resolution Observations

ID	Julian Date ^a $v_r(\text{km s}^{-1})^b$	Julian Date ^a $v_r(\text{km s}^{-1})^b$	Julian Date ^a $v_r(\text{km s}^{-1})^b$	Julian Date ^a $v_r(\text{km s}^{-1})^b$
HE0132–2429	1811.96 +296.0 (0.1)	3243.00 +289.5 (0.2)	3289.89 +289.2 (0.1)	
HE1012–1540	2396.82 +226.3 (0.4)	3489.77 +224.8 (0.1)		
HE1300+0157	2830.50 ^c +73.6 (2.0)	3157.74 ^d 74.6 (0.6)	3432.01 ^d 74.6 (0.6)	3843.87 +73.4 (0.1)
HE1346–1025	3149.80 +48.6 (0.5)	4198.92 +49.4 (0.1)		
HE1356–0622	3149.89 +93.5 (0.4)	3989.72 +94.1 (0.2)		
HE1424–0241	3152.90 +58.8 (0.6)	3844.96 +60.4 (0.1)		
HE2323–0256	1764.73 ^e –125.6 (0.1) ^e	2158.73 ^e –125.6 (0.1) ^e	2544.90 –125.9 (0.1)	3312.76 –125.9 (0.1)
BS16467–062	2064.55 ^e –90.6 (0.1)	2095.45 ^e –90.5 (0.1)	3490.02 –91.7 (0.1)	

^aJulian date – 2450000.00.

^bHeliocentric v_r and its 1σ uncertainty.

^c v_r from HERES/UVES (Barklem *et al.* 2005).

^d v_r from Subaru/HDS spectra of Frebel *et al.* (2007).

^e v_r provided by M.Spite & R.Cayrel (from UVES spectra).

Table 4. W_λ for the Sample EMP Stars From the HES

λ (Å)	Species	EP (eV)	$\log(gf)$	HE0132–2429 (mÅ)	HE1012–1540	HE1300+0157	HE1356–0622	HE1347–1025	HE1424–0241	BS16467–062	HE2323–0256
3189.30	OH	1.03	–1.990	≤21.2
3255.50	OH	1.30	–1.940	≤14.3	40.0
5889.95	Na I	0.00	0.110	62.8	168.8	48.2	132.8	64.9	65.7	50.1	192.7
5895.92	Na I	0.00	–0.190	50.4	146.7	26.8	117.3	52.2	39.0	27.8	159.2
3829.36	Mg I	2.71	–0.210	93.3	259.0	84.2	79.0	81.8	139.7
4057.52	Mg I	4.34	–1.200	...	22.0	...	9.0	22.6
4167.28	Mg I	4.34	–1.000	10.5	6.8	28.7
4703.00	Mg I	4.34	–0.670	9.0	72.2	...	24.4	16.0	47.5
5172.70	Mg I	2.71	–0.380	101.3	301.2	92.6	128.2	110.5	89.7	92.7	160.6
5183.62	Mg I	2.72	–0.160	114.3	391.5	103.7	142.2	120.8	104.7	105.2	179.9
5528.40	Mg I	4.34	–0.480	12.1	59.3	48.3
3944.01	Al I	0.00	–0.640	39.1	61.5	58.5	23.0	34.2	123.8
3961.52	Al I	0.00	–0.340	42.7	103.0	36.4	76.8	62.5	27.1	37.1	89.7
3905.53	Si I	1.91	–1.040	110.5	133.7	93.5	141.7	116.5	16.0	93.4	150.7
4102.94	Si I	1.91	–3.140	41.3	8.0	13.7
4226.74	Ca I	0.00	0.240	105.7	...	94.1	134.0	111.1	58.7	98.8	116.6
4289.37	Ca I	1.88	–0.300	16.9	9.8
4302.54	Ca I	1.90	0.280	22.6	39.5	32.4	...	12.0	...
4318.66	Ca I	1.90	–0.210	16.3
4425.44	Ca I	1.88	–0.360	14.0	9.0
4435.69	Ca I	1.89	–0.520	...	7.3	...	13.0
4454.79	Ca I	1.90	0.260	17.4	21.3	15.9	36.2	26.7	...	17.2	82.0
3736.90	Ca II	3.15	–0.148	75.0	50.9	69.7	44.0	70.8	...
4246.82	Sc II	0.32	0.242	79.3	...	30.9	87.6	43.3	20.5	43.3	63.8
4314.08	Sc II	0.62	–0.100	43.1	49.5	20.0	...	13.4	...
4320.73	Sc II	0.60	–0.260	33.6	36.8	11.1	...
4670.41	Sc II	1.36	–0.580	7.5
3958.22	Ti I	0.05	–0.160	15.3	18.9	<13.5
3998.64	Ti I	0.05	–0.050	13.5	24.7	<25.0	...	9.6	...
4533.25	Ti I	0.85	0.480	14.0	<16.0
4534.78	Ti I	0.84	0.280	11.0
4981.74	Ti I	0.85	0.500	12.0	18.0	<12.0	...	4.9	...
4999.51	Ti I	0.83	0.250	...	<6.0	<10.0
3900.54	Ti II	1.13	–0.450	52.2	13.6	27.9	76.5	54.1	14.0	41.6	61.1
3987.61	Ti II	0.61	–2.730	5.0
4012.39	Ti II	0.57	–1.610	24.4	46.8	23.7	8.5	20.3	31.4
4028.35	Ti II	1.89	–0.870	5.3	14.0
4300.05	Ti II	1.18	–0.490	42.6	67.2	46.6	7.5	30.9	...
4301.93	Ti II	1.16	–1.200	17.9	37.6	10.3	...
4312.86	Ti II	1.18	–1.160	23.4	41.0	23.7	...	8.5	...
4395.03	Ti II	1.08	–0.510	49.5	...	24.4	76.4	56.7	12.0	39.5	60.6
4399.77	Ti II	1.24	–1.290	19.9	31.6	17.5	...	12.1	20.2
4417.72	Ti II	1.16	–1.160	23.0	38.6	31.3	...	12.1	25.4
4443.81	Ti II	1.08	–0.700	44.0	11.8	20.3	69.8	51.1	...	39.9	58.2
4468.51	Ti II	1.13	–0.600	46.8	19.9	22.1	74.3	50.3	10.7	31.2	53.8
4501.28	Ti II	1.12	–0.760	41.7	11.2	20.7	66.8	49.9	12.2	31.9	51.4
4533.97	Ti II	1.24	–0.640	37.4	14.0	15.5	63.5	42.2	8.3	24.8	49.3
4563.77	Ti II	1.22	–0.820	30.1	10.6	13.4	56.1	32.3	5.1	24.7	39.5
4571.98	Ti II	1.57	–0.340	33.4	13.7	17.3	58.5	28.9	...	19.7	42.8

Table 4—Continued

λ (Å)	Species	EP (eV)	$\log(gf)$	HE0132–2429 (mÅ)	HE1012–1540	HE1300+0157	HE1356–0622	HE1347–1025	HE1424–0241	BS16467–062	HE2323–0256
4589.95	Ti II	1.24	–1.650	15.5
4111.77	V I	0.30	0.408	<5.6
3545.19	V II	1.10	–0.390	<10.9	11.6	11.8
3592.03	V II	1.10	–0.370	12.4	8.2	11.5
4254.33	Cr I	0.00	–0.110	31.5	...	21.5	58.9	40.6	23.6	30.6	38.4
4274.79	Cr I	0.00	–0.230	29.2	...	16.8	47.3	32.5	19.7	22.5	29.3
4289.72	Cr I	0.00	–0.361	22.8	42.3	26.5	13.4	20.0	31.8
5206.04	Cr I	0.94	0.030	11.9	8.4	4.7	23.2	14.0	5.8	6.2	7.4
5208.43	Cr I	0.94	0.158	14.3	8.5	7.6	7.7	12.8	18.2
4030.75	Mn I	0.00	–0.470	17.3	20.0	10.8	36.6	26.0	34.7	17.4	22.1
4033.06	Mn I	0.00	–0.620	12.3	15.0	8.5	30.0	18.0	26.3	14.4	17.9
3441.99	Mn II	1.78	–0.273	28.0	10.0	16.2	48.4	32.0	...
3460.32	Mn II	1.81	–0.540	23.5	...	14.3	37.9	20.4	32.3
3488.68	Mn II	1.85	–0.860	15.9	29.8	13.0	...
3865.52	Fe I	1.01	–0.980	63.8	46.5	48.8	88.1	74.2	50.2	66.2	72.8
3886.29	Fe I	0.05	–1.080	90.5
3887.06	Fe I	0.91	–1.140	40.5
3895.67	Fe I	0.11	–1.670	79.4	...	69.2	101.9	83.4	69.4	78.6	96.4
3899.72	Fe I	0.09	–1.530	83.7	70.2	72.9	115.0	92.1	73.5	84.6	95.8
3902.96	Fe I	1.56	–0.470	55.9	48.0	45.9	80.6	70.8	41.4	56.1	59.7
3906.49	Fe I	0.11	–2.240	60.7	36.0	41.8	92.4	73.9	47.5	60.7	68.3
3920.27	Fe I	0.12	–1.750	83.5	59.9	66.4	106.4	82.9	70.2	...	95.7
3922.92	Fe I	0.05	–1.650	90.5	58.1	74.1	113.3	95.4	79.4	85.6	98.4
3930.31	Fe I	0.09	–1.590	...	75.0	75.7
3949.96	Fe I	2.18	–1.160	8.6	18.2	9.2	8.5	8.6	12.6
4005.24	Fe I	1.56	–0.610	54.9	45.8	41.3	80.3	68.1	39.5	56.7	63.0
4045.81	Fe I	1.49	0.280	90.0	94.1	79.5	121.5	106.7	78.1	89.4	99.3
4063.59	Fe I	1.56	0.060	...	69.1	...	101.3	82.9
4071.74	Fe I	1.61	–0.020	...	68.3	...	99.6	83.8
4118.55	Fe I	3.57	0.140	18.0
4132.06	Fe I	1.61	–0.820	49.0	37.6	36.0	81.7	68.2	40.5	48.7	62.3
4143.87	Fe I	1.56	–0.620	57.8	42.6	47.7	84.9	66.8	49.6	60.2	65.9
4147.67	Fe I	1.49	–2.100	13.6	19.0	8.0	...	6.4	8.7
4172.76	Fe I	0.96	–3.070	7.1	6.0
4181.75	Fe I	2.83	–0.370	12.2	...	7.3	21.5	17.1	...	14.4	13.3
4187.05	Fe I	2.45	–0.550	35.4	19.1	16.1	14.4	19.2
4187.81	Fe I	2.43	–0.550	12.6	38.8	27.9	13.2	20.0	25.0
4198.33	Fe I	2.40	–0.720	33.4	20.0	...	12.4	20.2
4199.10	Fe I	3.05	0.160	14.0	...	14.5	31.8	22.3	...	16.3	25.3
4202.04	Fe I	1.49	–0.710	59.1	...	45.9	80.6	65.0	47.2	59.5	67.3
4216.19	Fe I	0.00	–3.360	18.2	41.2	19.9	8.2	20.1	23.5
4222.22	Fe I	2.45	–0.970	7.8	...
4227.44	Fe I	3.33	0.270	15.1	...	11.9	11.2	15.3
4233.61	Fe I	2.48	–0.600	17.7	32.4	22.0	...	14.3	18.7
4235.95	Fe I	2.43	–0.340	26.4	44.2	32.2	11.6	39.4	...
4250.13	Fe I	2.47	–0.410	16.6	...	15.9	44.6	25.2	...	20.6	22.1
4250.80	Fe I	1.56	–0.380	54.3	...	39.5	76.0	53.3	39.4	49.4	64.0
4260.49	Fe I	2.40	0.140	41.0	...	29.0	64.9	48.3	28.2	41.6	44.4
4271.16	Fe I	2.45	–0.350	30.1	...	15.0	41.5	29.3	11.8	18.1	26.5
4271.77	Fe I	1.49	–0.160	74.9	...	61.5	94.3	83.4	60.6	74.4	81.9

Table 4—Continued

λ (Å)	Species	EP (eV)	$\log(gf)$	HE0132–2429 (mÅ)	HE1012–1540	HE1300+0157	HE1356–0622	HE1347–1025	HE1424–0241	BS16467–062	HE2323–0256
4282.41	Fe I	2.18	−0.780	19.9	38.6	20.0	19.5
4294.14	Fe I	1.49	−0.970	51.6	83.1	57.4	...	46.3	66.1
4299.25	Fe I	2.43	−0.350	25.8	47.8	47.3	15.0	20.4	...
4307.91	Fe I	1.56	−0.070	85.0	97.6	68.9	84.2	...
4325.77	Fe I	1.61	0.010	76.0	102.6	80.2	60.8	72.8	...
4337.05	Fe I	1.56	−1.690	21.5	41.9	25.5	28.3
4375.94	Fe I	0.00	−3.030	32.1	...	17.4	67.7	34.6	19.7	30.8	36.9
4383.56	Fe I	1.49	0.200	96.7	...	79.2	126.2	99.0	78.9	86.1	96.9
4404.76	Fe I	1.56	−0.140	75.1	64.3	66.0	100.9	86.2	62.5	72.9	83.4
4415.13	Fe I	1.61	−0.610	51.9	43.9	45.3	81.1	65.3	46.5	58.5	62.0
4427.32	Fe I	0.05	−3.040	33.6	...	15.9	59.6	39.7	...	30.5	40.0
4442.35	Fe I	2.20	−1.250	9.0	...	7.2	24.0	...	6.6	8.5	16.2
4447.73	Fe I	2.22	−1.340	13.7	9.1
4459.14	Fe I	2.18	−1.280	5.2	8.8
4461.66	Fe I	0.09	−3.210	22.1	17.5	16.4	52.1	30.6	10.2	26.6	29.0
4489.75	Fe I	0.12	−3.970	12.6	5.0
4494.57	Fe I	2.20	−1.140	19.6	...	9.7	23.4	16.8	8.9	10.9	17.8
4531.16	Fe I	1.49	−2.150	6.2	17.5	5.0
4592.66	Fe I	1.56	−2.450	9.1	5.0
4602.95	Fe I	1.49	−2.220	7.8	16.2	5.0
4871.33	Fe I	2.86	−0.360	11.9	10.6	...	24.9	9.8	...	18.7	18.0
4872.14	Fe I	2.88	−0.570	6.7	8.0	...	18.0	4.6	11.2
4891.50	Fe I	2.85	−0.110	19.0	21.5	17.5	35.3	23.4	23.9
4919.00	Fe I	2.86	−0.340	...	10.0	...	22.5	14.0	...	8.5	10.1
4920.51	Fe I	2.83	0.150	17.4	16.5	13.1	36.2	26.0	9.9	19.9	22.3
4957.61	Fe I	2.81	0.230	34.3	31.7	26.0	56.1	37.5	22.0	...	37.7
5083.34	Fe I	0.96	−2.960	17.6
5166.28	Fe I	0.00	−4.200	11.5
5171.61	Fe I	1.48	−1.790	19.2	17.9	13.2	38.2	27.4	...	13.0	...
5192.35	Fe I	3.00	−0.420	6.1	14.4
5194.95	Fe I	1.56	−2.090	18.0	7.8	...
5216.28	Fe I	1.61	−2.150	12.8	6.5
5227.19	Fe I	1.56	−1.350	36.4	21.8	24.8	62.8	45.9	...	34.6	46.6
5232.95	Fe I	2.94	−0.100	15.5	15.0	...	30.4	...	5.6	16.4	17.9
5269.55	Fe I	0.86	−1.320	75.8	55.8	55.7	103.1	97.3	61.8	76.6	85.6
5324.19	Fe I	3.21	−0.100	14.6	6.8	...
5405.79	Fe I	0.99	−1.840	39.3	25.5	25.7	27.5	38.8	46.3
5434.53	Fe I	1.01	−2.130	19.7	7.0	21.7	23.6
5506.79	Fe I	0.99	−2.790	6.8	...
3255.90	Fe II	0.99	−2.498	49.6	36.4	33.6	50.4	54.2	71.2
3277.36	Fe II	0.99	−2.191	52.3	52.1	46.6	53.4	58.6	74.5
3281.30	Fe II	1.04	−2.678	41.0	28.7	24.8	34.6	45.0	...
4178.86	Fe II	2.57	−2.530	16.6	10.2	...	5.1	...
4233.17	Fe II	2.57	−2.000	13.9	...	9.0	40.5	...	12.0	17.8	22.7
4416.82	Fe II	2.77	−2.430	10.8	4.1
4508.30	Fe II	2.84	−2.280	5.2	10.8	6.8
4555.89	Fe II	2.82	−2.170	14.4	16.8	6.8
4583.84	Fe II	2.81	−2.020	10.5	30.5	15.0	...	8.6	17.4
4923.93	Fe II	2.88	−1.320	17.5	5.2	12.6	45.8	17.7	25.2
5018.45	Fe II	2.89	−1.220	26.6	7.8	16.5	58.6	36.6	12.6	24.6	35.1

Table 4—Continued

λ (Å)	Species	EP (eV)	$\log(gf)$	HE0132–2429 (mÅ)	HE1012–1540	HE1300+0157	HE1356–0622	HE1347–1025	HE1424–0241	BS16467–062	HE2323–0256
3842.05	Co I	0.92	−0.763	9.0	18.0
3845.46	Co I	0.92	0.009	19.9	10.3	16.5	36.8	33.4	28.0	25.6	26.8
3873.11	Co I	0.43	−0.666	29.7	...	9.6	41.7	40.0	34.8	43.9	38.8
4121.31	Co I	0.92	−0.315	19.8	...	9.9	25.0	18.2	26.0	25.3	23.1
3807.15	Ni I	0.42	−1.180	41.4	16.5	29.0	58.9	45.3	42.7	49.0	41.4
3858.30	Ni I	0.42	−0.967	56.6	29.8	41.7	79.2	56.5	53.0	60.8	55.5
4401.55	Ni I	3.19	0.084	7.0
3247.53	Cu I	0.00	−0.060	26.0	...	22.6	30.8	... ^a
3273.95	Cu I	0.00	−0.360	18.4	13.0	14.4	13.9	20.0	25.5
4810.54	Zn I	4.08	−0.170	<4.5	<5.0	<6.0	...	<5.0	...
4077.71	Sr II	0.00	0.170	82.9	44.4	...	27.6	37.2	<5.0	...	106.1
4215.52	Sr II	0.00	−0.140	75.6	...	4.8	13.3	34.2	<5.0	5.2	96.1
4554.04	Ba II	0.00	0.170	8.4	13.7	<5.5	22.2	21.5	4.5	<4.3	19.7
4934.16	Ba II	0.00	−0.150	5.2	8.3	<5.5	7.0	12.6	...	<5.0	21.7
5853.70	Ba II	0.60	−1.010	<2.0	...
3774.33	Y II	0.13	0.220	<10.0
3950.36	Y II	0.10	−0.490	<6.9	<9.0	...	<4.5
3819.67	Eu II	0.00	0.510	<8.0	<7.5
3971.96	Eu II	0.21	0.270	<4.5
4129.70	Eu II	0.00	0.220	<8.0	<8.0	...	<9.0	<15.0	<5.0
3407.80	Dy II	0.00	0.180	<16.1
3531.71	Dy II	0.00	0.770	<8.8
4057.81	Pb I	1.32	−0.220	...	<8.0

^aToo blended to use.

Table 5. Fit Fe I Slopes With EP, Equivalent Width, and Wavelength

Star ID	$\Delta[\text{X}/\text{Fe}]/\Delta(\text{EP})^{\text{a}}$ (dex/eV)	$\Delta[\text{X}/\text{Fe}]/\Delta[W_{\lambda}/\lambda]$ (dex)	$\Delta[\text{X}/\text{Fe}]/\Delta\lambda$ ($10^{-4}\text{dex}/\text{\AA}$)
C-normal			
HE0132–2429	–0.068	–0.074	+0.09
HE1347–1025	–0.044	–0.007	+0.32
HE1356–0622	–0.053	–0.136	+0.33
HE1424–0241	–0.041	–0.079	–0.32
BS16467–062	–0.091	+0.076	–0.05
C-rich			
HE1012–1540	+0.014	–0.091	+0.71
HE1300+0157	–0.098	+0.022	+0.11
HE2323–0256	–0.036	+0.005	–0.67

^aTypical range of EP is 3 eV. Often only the 0 eV lines are discrepant.

Table 6. Abundances for the Five C-Normal EMP Stars From the HES

Species	HE0132-2429 [Fe/H] -3.55				HE1347-1025 [Fe/H] -3.48				HE1356-0622 [Fe/H] -3.49				HE1424-0241 [Fe/H] -3.96				BS16467-062 [Fe/H] -3.47			
	[X/Fe] (dex)	log $\epsilon(X)$ (dex)	No. Lines	σ (dex)	[X/Fe] (dex)	log $\epsilon(X)$ (dex)	No. Lines	σ (dex)	[X/Fe] (dex)	log $\epsilon(X)$ (dex)	No. Lines	σ (dex)	[X/Fe] (dex)	log $\epsilon(X)$ (dex)	No. Lines	σ (dex)	[X/Fe] (dex)	log $\epsilon(X)$ (dex)	No. Lines	σ (dex)
C(CH)	0.62	5.66	1	...	0.15	5.26	1	...	≤ -0.05	≤ 5.06	1	...	≤ 0.63	≤ 5.26	1	...	0.48	5.60	1	...
N(NH)	1.07	5.45	1	≤ 1.13	≤ 5.10	1	...	≤ 0.54	≤ 5.00	1	...
O(OH)	≤ 1.67	≤ 6.95	2	0.20	≤ 1.79	≤ 7.15	2	0.20
Na I	-0.31	2.46	2	0.09	-0.42	2.42	2	0.08	0.31	3.15	2	0.03	-0.04	2.32	2	0.07	-0.60	2.25	2	0.07
Mg I	0.40	4.39	5	0.15	0.49	4.55	3	0.22	0.67	4.72	5	0.32	0.45	4.03	3	0.12	0.31	4.37	4	0.33
Al I	-0.19	2.74	2	0.17	-0.02	2.97	2	0.17	-0.13	2.86	2	0.05	-0.16	2.35	2	0.15	-0.28	2.72	2	0.18
Si I	0.57	4.57	1	...	0.41	4.48	2	0.23	0.81	4.88	2	0.16	-1.00	2.59	1	...	0.27	4.35	1	...
Ca I	0.27	3.08	3	0.15	0.36	3.24	5	0.18	0.43	3.31	7	0.17	-0.56	1.84	1	...	0.12	3.00	3	0.12
Ca II	0.00	2.81	1	-0.30	2.10	1	...	-0.02	2.87	1	...
Sc II	0.75	0.31	3	0.05	0.00	-0.38	2	0.12	0.32	-0.06	4	0.17	-0.08	-0.94	1	...	0.16	-0.22	3	0.03
Ti I	0.61	2.05	3	0.10	≤ 0.62	≤ 2.13	4	0.09	0.40	1.91	5	0.06	0.28	1.80	2	0.09
Ti II	0.39	1.84	15	0.10	0.26	1.77	13	0.11	0.26	1.76	17	0.07	-0.17	0.85	8	0.17	0.20	1.72	14	0.12
V I	≤ 0.69	≤ 1.21	1
V II	0.36	0.81	1	≤ 0.60	≤ 0.64	1	...	0.28	0.81	2	0.14
Cr I	-0.43	1.69	5	0.12	-0.52	1.67	4	0.11	-0.52	1.66	4	0.13	-0.38	1.33	5	0.09	-0.54	1.65	5	0.10
Mn I ^b	-0.90	0.94	2	0.02	-0.88	1.03	2	0.04	-0.98	0.92	2	0.02	-0.10	1.33	2	0.02	-0.85	1.06	2	0.04
Mn II	-0.48	1.37	3	0.16	0.19	1.62	3	0.13	-0.48	1.44	3	0.07
Fe I	-3.55 ^a	3.90	53	0.18	-3.48	3.97	50	0.22	-3.49	3.96	63	0.16	-3.96	3.49	39	0.18	-3.47	3.98	57	0.19
Fe II	-0.05	3.85	8	0.18	0.20	4.17	4	0.19	0.13	4.10	8	0.13	0.09	3.58	5	0.19	0.04	4.01	8	0.16
Co I	0.55	1.92	4	0.18	0.48	1.92	3	0.19	0.24	1.67	3	0.11	1.03	1.98	4	0.21	0.68	2.12	3	0.28
Ni I	-0.04	2.67	2	0.06	-0.19	2.58	1	...	-0.04	2.72	3	0.33	0.24	2.52	2	0.01	0.15	2.93	2	0.04
Cu I	-0.85	-0.18	2	0.06	-0.66	-0.41	1	...	-0.75	-0.01	2	0.01
Zn I	≤ 0.84	≤ 1.89	1	...	≤ 0.94	≤ 2.06	2	0.17	≤ 0.55	≤ 1.66	1	≤ 0.96	≤ 2.09	2	0.12
Sr II	0.05	-0.60	2	0.06	-1.13	-1.71	2	0.16	-1.88	-2.47	2	0.08	≤ -1.69	≤ -2.75	2	0.21	-1.75	-2.32	1	...
Y II	≤ 0.33	≤ -0.98	1	≤ -0.13	≤ -1.38	1	...	≤ 0.26	≤ -1.46	2	0.19
Ba II	-0.85	-2.27	2	0.04	-0.62	-1.96	2	0.01	-1.19	-2.54	2	0.21	-0.91	-2.74	1	...	≤ -0.56	≤ -1.91	3	0.72
Eu II	≤ 1.18	≤ -1.86	2	0.18	≤ 1.39	≤ -1.58	1	...	≤ 0.56	≤ -2.41	3	0.18	≤ 1.50	≤ -1.95	1
Dy II	≤ 1.56	≤ -1.30	2

^a[Fe I/H] is given instead of [X/Fe].^bA correction of +0.3 dex to [Mn/Fe] as derived from lines of the 4030 Å Mn I triplet is required, but not put in here. See §5.

Table 7. Abundances for the Three C-Rich EMP Stars From the HES

Species	HE1012–1540 [Fe/H] –3.43				HE1300+0157 [Fe/H] –3.39				HE2323–0256 [Fe/H] –3.79			
	[X/Fe] (dex)	$\log\epsilon(X)$ (dex)	No. Lines	σ (dex)	[X/Fe] (dex)	$\log\epsilon(X)$ (dex)	No. Lines	σ (dex)	[X/Fe] (dex)	$\log\epsilon(X)$ (dex)	No. Lines	σ (dex)
C(CH)	2.22	7.38	1	...	1.23	6.43	1	...	0.97	5.77	1	...
N(NH)	1.25	5.75	1	...	<0.71	<5.25	1	...	2.16	6.30	2	0.30
O(OH)	2.25	7.65	2	0.25	1.69	7.13	2	0.18	1.96	7.20	1	...
Na I	1.21	4.11	2	0.07	–0.49	2.44	2	0.07	1.45	3.98	2	0.11
Mg I	1.88	5.99	6	0.44	0.32	4.47	3	0.10	1.47	5.22	7	0.25
Al I	0.93	3.97	1	...	–0.24	2.83	1	...	0.48	3.16	1	...
Si I	1.07	5.20	1	...	0.49	4.64	1	...	0.56	4.32	1	...
Ca I	0.57	3.50	2	0.16	0.26	3.23	2	0.13	0.31	2.88	2	0.11
Ca II	–0.34	2.59	1	...	0.10	3.07	1	...	0.08	2.65	1	...
Sc II	0.17	–0.12	1	...	0.12	–0.56	1	...
Ti I	<0.75	<2.31	1	<0.46	<1.66	1	...
Ti II	–0.03	1.53	7	0.12	0.12	1.72	8	0.06	0.27	1.47	11	0.06
V II	0.09	0.30	2	0.03
Cr I	–0.33	1.91	2	0.09	–0.53	1.74	4	0.07	–0.54	1.34	5	0.15
Mn I ^a	–0.55	1.41	2	0.01	–0.86	1.13	2	0.02	–0.97	0.63	2	0.03
Mn II	–1.00	0.96	1	...	–0.66	1.33	2	0.16	–0.43	1.17	2	0.01
Fe I	–3.43 ^b	4.02	28	0.17	–3.39 ^b	4.06	36	0.19	–3.79 ^b	3.66	57	0.16
Fe II	–0.28	3.75	5	0.35	–0.16	3.90	6	0.11	0.06	3.72	9	0.18
Co I	0.19	1.68	1	...	0.39	1.92	3	0.08	0.42	1.55	3	0.18
Ni I	–0.32	2.50	2	0.09	–0.02	2.83	2	0.06	–0.26	2.20	2	0.04
Cu I	–0.63	0.15	1	...	–0.68	0.13	2	0.02	–0.78	–0.36	1	...
Sr II	–0.54	–1.07	1	...	–1.55	–2.05	1	...	0.18	–0.71	2	0.02
Ba II	–0.29	–1.58	2	0.02	< –0.63	< –1.89	2	0.20	–0.66	–2.32	2	0.23
Eu II	<1.62	< –1.30	1	<0.73	< –2.55	1	...
Pb I	<2.93	<1.46	1

^aA correction of +0.3 dex to [Mn/Fe] as derived from lines of the 4030 Å Mn I triplet is required, but not put in here. See §5.

^b[Fe I/H] is given instead of [X/Fe].

Table 8. Abundance Range for Five C-normal EMP Stars From the HES

Species [X/Fe]	Nu. stars (dex)	Mean [X/Fe] (dex)	σ (dex)	Min. (dex)	Max. (dex)
[C(CH)/Fe] ^a	3	0.39	0.29	0.07	0.62
[N(NH)/Fe] ^b					
[O(OH)/Fe] ^c					
[Na/Fe] ^d	5	−0.21	0.36	−0.60	0.32
[Mg/Fe]	5	0.46	0.13	0.31	0.67
[Al/Fe] ^e	5	−0.16	0.09	−0.28	−0.02
[Si/Fe]	5	0.21	0.71	−1.00	0.81
[CaI/Fe]	5	0.12	0.40	−0.56	0.43
[CaII/Fe]	3	−0.11	0.17	−0.30	0.00
[Sc/Fe]	5	0.23	0.33	−0.08	0.75
[Ti/Fe] ^f	5	0.19	0.21	−0.17	0.40
[V/Fe]	2	0.32	0.05	0.28	0.36
[Cr/Fe]	5	−0.48	0.07	−0.54	−0.38
[MnI/Fe] ^g	5	−0.75	0.36	−0.99	−0.10
[MnII/Fe]	3	−0.26	0.39	−0.48	0.19
[FeII/FeI]	5	0.08	0.10	−0.05	0.20
[Co/Fe]	5	0.59	0.29	0.24	1.03
[Ni/Fe]	5	0.02	0.17	−0.19	0.24
[Cu/Fe]	3	−0.75	0.09	−0.85	−0.66
[Sr/Fe]	4	−1.18	0.88	−1.88	0.05
[Ba/Fe]	4	−0.89	0.24	−1.19	−0.62

^aTwo stars only have upper limits for [C/Fe].

^bOne detection and two upper limits for [N/Fe].

^cTwo upper limits for [O/Fe].

^dNon-LTE correction of −0.2 dex has been applied for [Na/Fe] from the Na D lines.

^eNon-LTE correction of +0.6 dex has been applied for [Al/Fe] from the 3950 Å doublet.

^fFrom Ti II lines

^gA correction of +0.3 dex to [Mn/Fe] as derived from lines of the 4030 Å Mn I triplet is required, but not put in here. See §5.

Table 9. Abundance Range for Three C-rich EMP Stars From the HES

Species [X/Fe]	Nu. stars (dex)	Mean [X/Fe] (dex)	σ (dex)	Min. (dex)	Max.
[C/Fe]	3	1.47	0.66	0.97	2.22
[N/Fe]	2	1.37	0.70	0.64	2.15
[O/Fe]	3	2.03	0.30	1.69	2.25
[Na/Fe] ^a	3	0.72	1.06	−0.49	1.45
[Mg/Fe]	3	1.22	0.81	0.32	1.88
[Al/Fe] ^b	3	0.39	0.59	−0.24	0.93
[Si/Fe]	3	0.71	0.32	0.49	1.08
[CaI/Fe]	3	0.38	0.17	0.26	0.57
[CaII/Fe]	2	−0.12	0.32	−0.34	0.10
[Sc/Fe]	2	0.14	0.04	0.12	0.17
[Ti/Fe] ^c	3	0.12	0.15	−0.03	0.27
[Cr/Fe]	3	−0.41	0.12	−0.54	−0.33
[MnI/Fe] ^d	3	−0.80	0.22	−0.97	−0.55
[MnII/Fe]	3	−0.70	0.28	−1.00	−0.43
[FeII/FeI]	3	−0.12	0.17	−0.28	0.06
[Co/Fe]	3	0.33	0.12	0.19	0.42
[Ni/Fe]	3	−0.20	0.16	−0.32	−0.02
[Cu/Fe]	3	−0.70	0.08	−0.78	−0.63
[Sr/Fe]	3	−0.64	0.87	−1.55	0.17
[Ba/Fe]	2	−0.52	0.21	−0.66	−0.29

^aNon-LTE correction of −0.2 dex has been applied for [Na/Fe] from the Na D lines.

^bNon-LTE correction of +0.6 dex has been applied for [Al/Fe] from the 3950 Å doublet.

^cFrom Ti II lines

^dA correction of +0.3 dex to [Mn/Fe] as derived from lines of the

4030 Å Mn I triplet is required, but not put in here. See §5.

Table 10. Comparison of Detailed Abundance Analyses for HE1300+0157

$\log[\epsilon(X)]$	Frebel <i>et al.</i> (2007) (5450,3.2) (dex)	0Z/Frebel ^a (5450, 3.2) (dex)	0Z (5632,3.37) (dex)
[Fe/H]	−3.73	−3.60	−3.39
C(CH)	5.89	6.02	6.43
N(NH)	< 5.12	< 4.93	< 5.25
O(OH)	6.54	6.78	7.13
Na I ^b	2.44	2.49	2.64
Mg I	4.10	4.30	4.47
Al I ^c	2.64	2.66	2.83
Si I	4.50	4.44	4.65
Ca I	2.98	3.06	3.23
Ca II	2.75	2.96	3.07
Sc II	−0.37	−0.30	−0.12
Ti II	1.77	1.58	1.72
Cr I	1.51	1.56	1.74
Mn I ^d	0.65	0.91	1.13
Mn II	0.89	1.20	1.33
Fe I	3.72	3.85	4.06
Fe II	3.57	3.77	3.90
Co I	1.80	1.71	1.92
Ni I	2.61	2.61	2.83
Cu I	...	−0.10	0.13
Sr II	< −2.64	−2.22	−2.05
Ba II	< −2.56	< −2.08	< −1.89

^aThe stellar parameters are those of Frebel *et al.* (2007), but the analysis is that of our 0Z project with our own set of W_λ .

^bno non-LTE correction has been applied for [Na/Fe].

^cNon-LTE correction of +0.6 dex has been applied for [Al/Fe] from the 3950 Å doublet.

^dIn all cases only lines from the 4030 Å triplet of Mn I have been used. No correction factor has been added here. The +0.4 dex correction factor added by Frebel *et al.* (2007) has been removed.

Table 11. Comparison of T_{eff} For EMP Giants Between Our 0Z Survey and The First Stars Project

Star	$T_{\text{eff}}(0Z)$ (K)	$\Delta T_{\text{eff}}^{\text{Hybrid}^a}$ (K)	$\Delta T_{\text{eff}}[(\text{Cayrel } et al. 2004)$ – 0Z) (K)
CD –38 245	4830	–30	–30
BS16477–003	4928	–48	–28
HE2323–0256 ^b	4995 ^c	–65	–95
CS22948–066	5224	–96	–124
BS16467–062	5364	–66	–164

^aThe hybrid T_{eff} uses the codes of the 0Z project, but the reddening of the First Stars project, which is almost always slightly higher. In all cases, the V mag from Cayrel *et al.* (2004) is adopted. The value of $T_{\text{eff}}(\text{hybrid}) - T_{\text{eff}}(0Z)$ is given.

^bRediscovery of CS22949–037 from the HK Survey.

^c T_{eff} for this star adopted by the 0Z project is 4915 K as our observed V mag from ANDICAM is 14.41 mag, 0.05 mag fainter than that adopted by the First Stars project.

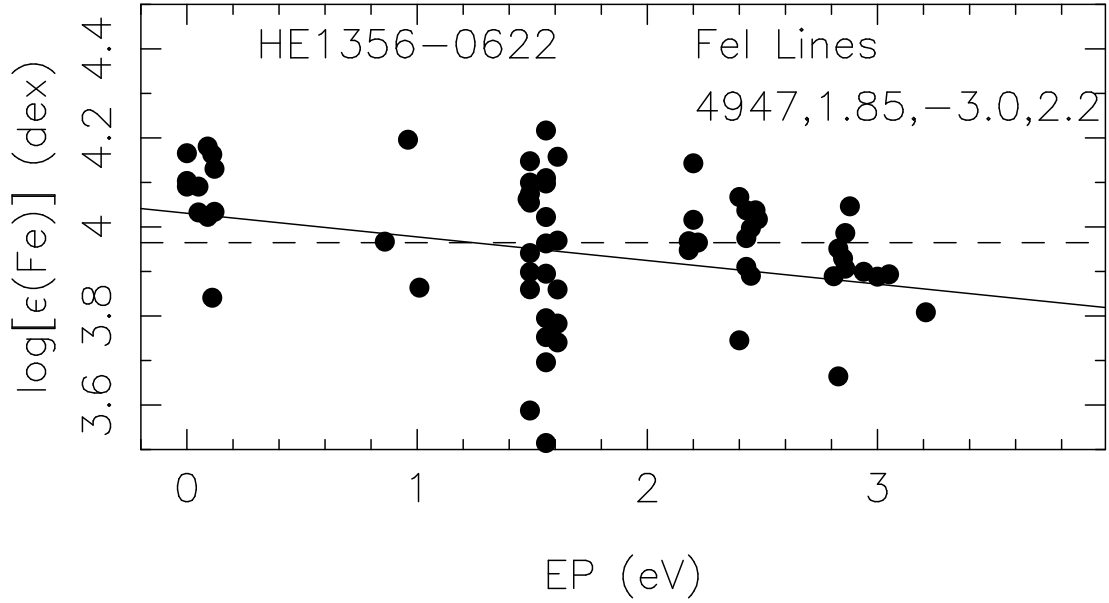


Fig. 1.— The iron abundance derived from each of the 63 Fe I lines seen in the spectrum of the EMP star HE1356–0622 is shown as a function of χ . The nominal set of stellar parameters we derive is used. The solid line is the linear fit, with slope -0.053 dex/eV with a modest correlation coefficient of -0.36 . However, only the 0 eV lines are discrepant. The dashed line indicates the mean $\log[\epsilon(\text{Fe})]$ derived from the 52 lines with $\chi > 0.2$ eV.

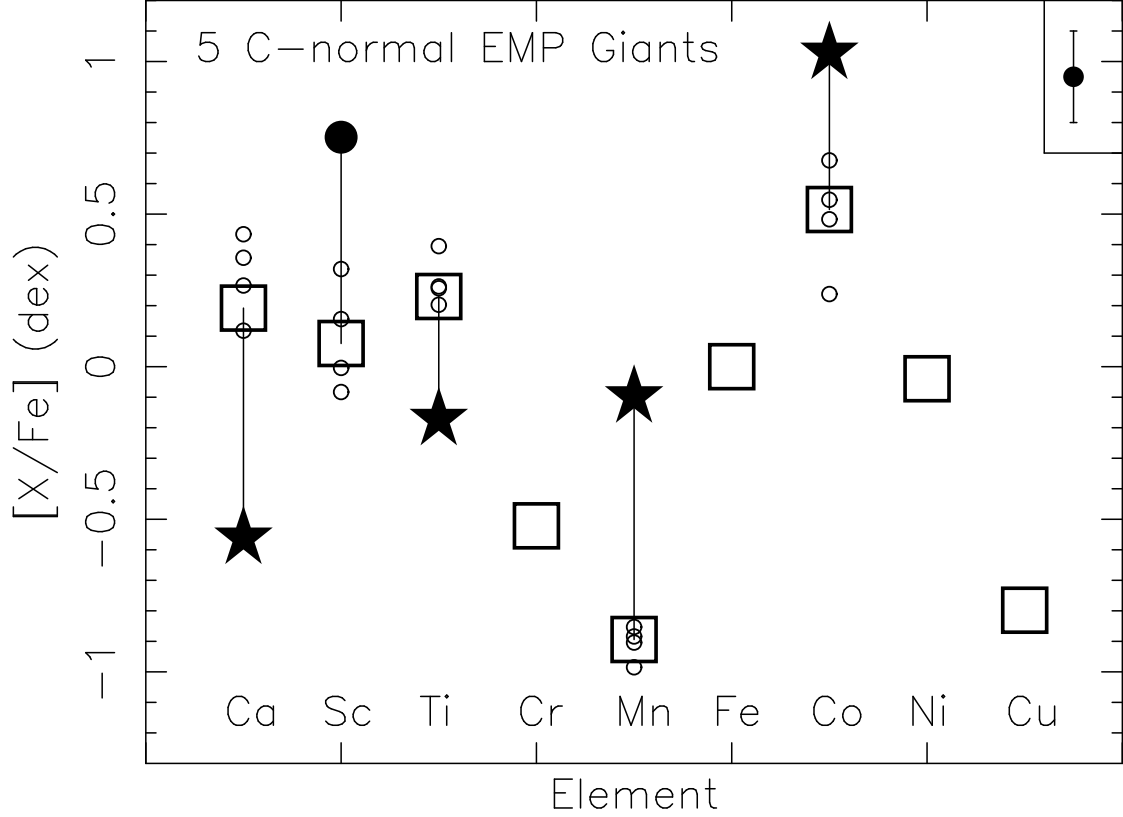


Fig. 2.— The median of $[X/Fe]$ for 9 elements from Ca to Cu is shown for the 5 C-normal stars as a box. Any ratio $[X/Fe]$ which differs from the median by more than 0.3 dex for HE1424–0241 is shown as a large star; the same for HE0132–2429 is shown as a large filled circle. If there is an outlier for a particular species, the abundance ratios for the remaining four C-normal EMP stars in our sample are shown as small open circles. A typical error bar for each ratio $[X/Fe]$ in a star is shown at the upper right.

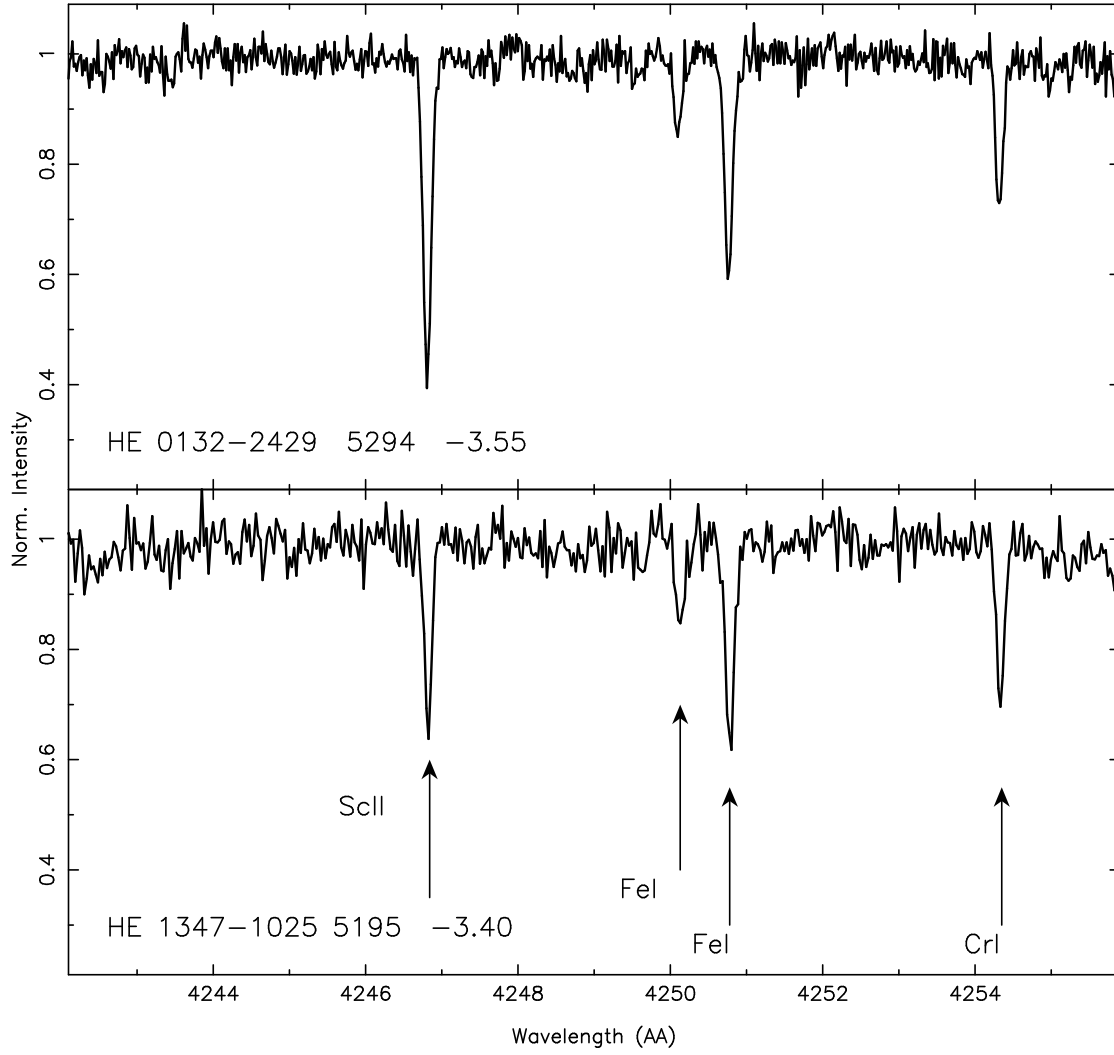


Fig. 3.— The region of the Sc II line at 4246 Å is shown in HE0132–2429 and in HE 1347–1025. $[\text{Fe}/\text{H}]$ differs for these two giants by only 0.15 dex, but the ScII line is much stronger in the former.

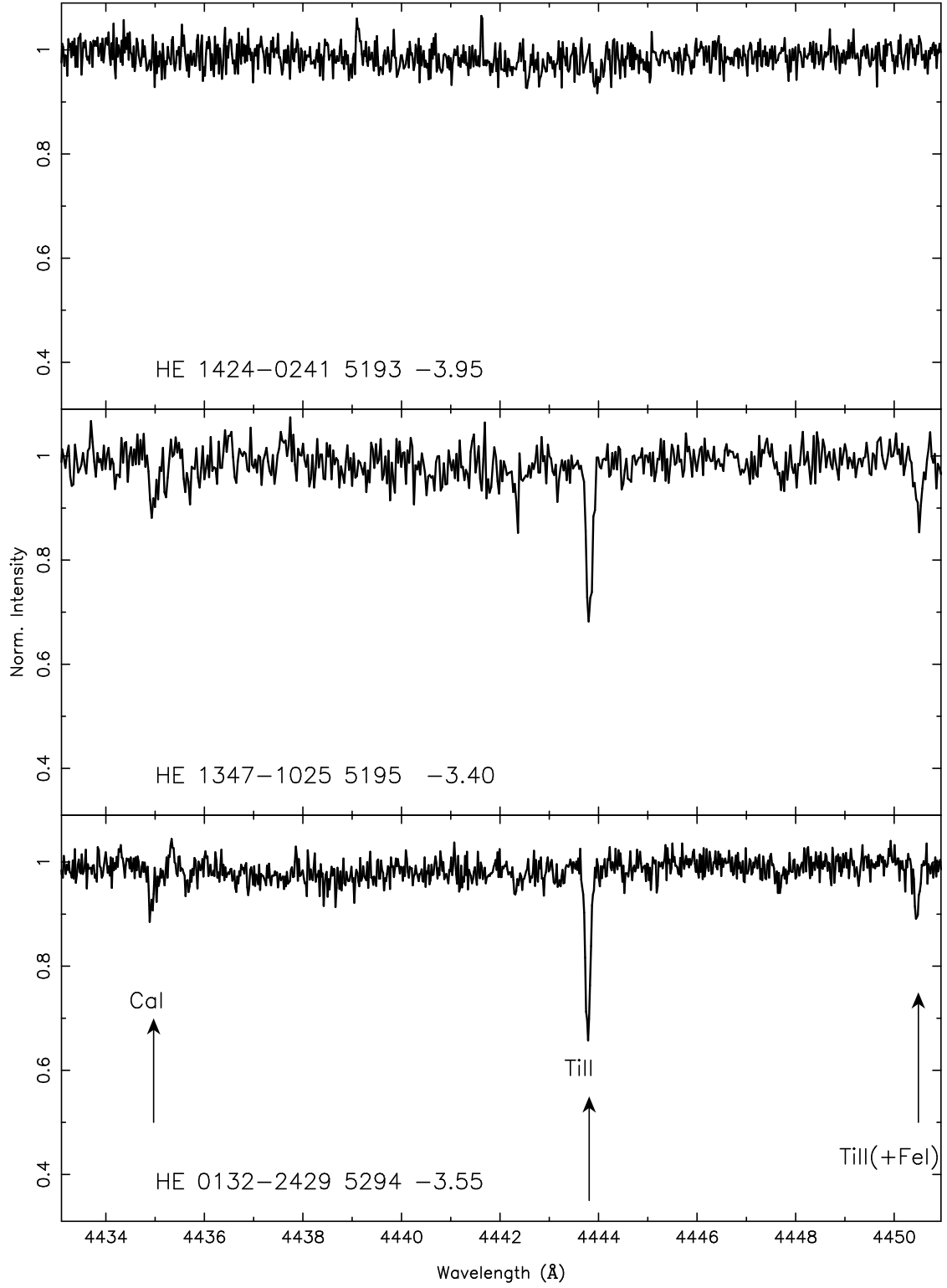


Fig. 4.— The region of the Ti II line at 4444 Å is shown in three of the C-normal EMP giants of our sample. The abnormally low $[\text{TiII}/\text{Fe}]$ ratio in HE1424–0241 is apparent.

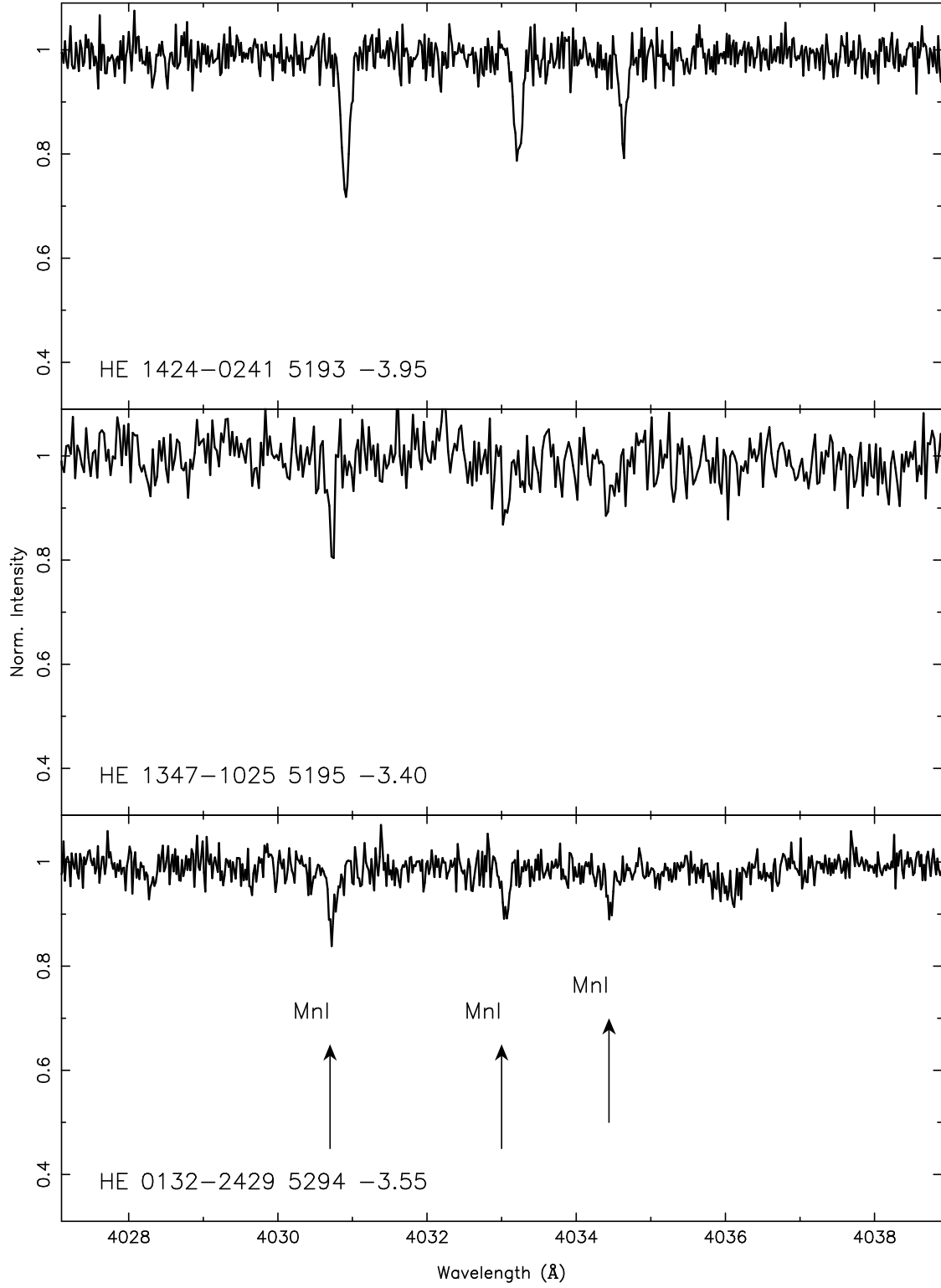


Fig. 5.— The region of the Mn I triplet at 4030 Å is shown in three of the C-normal EMP giants of our sample. The extremely high $[\text{Mn}/\text{Fe}]$ ratio in HE1424-0241 as compared to the other two stars whose spectra are displayed is apparent.

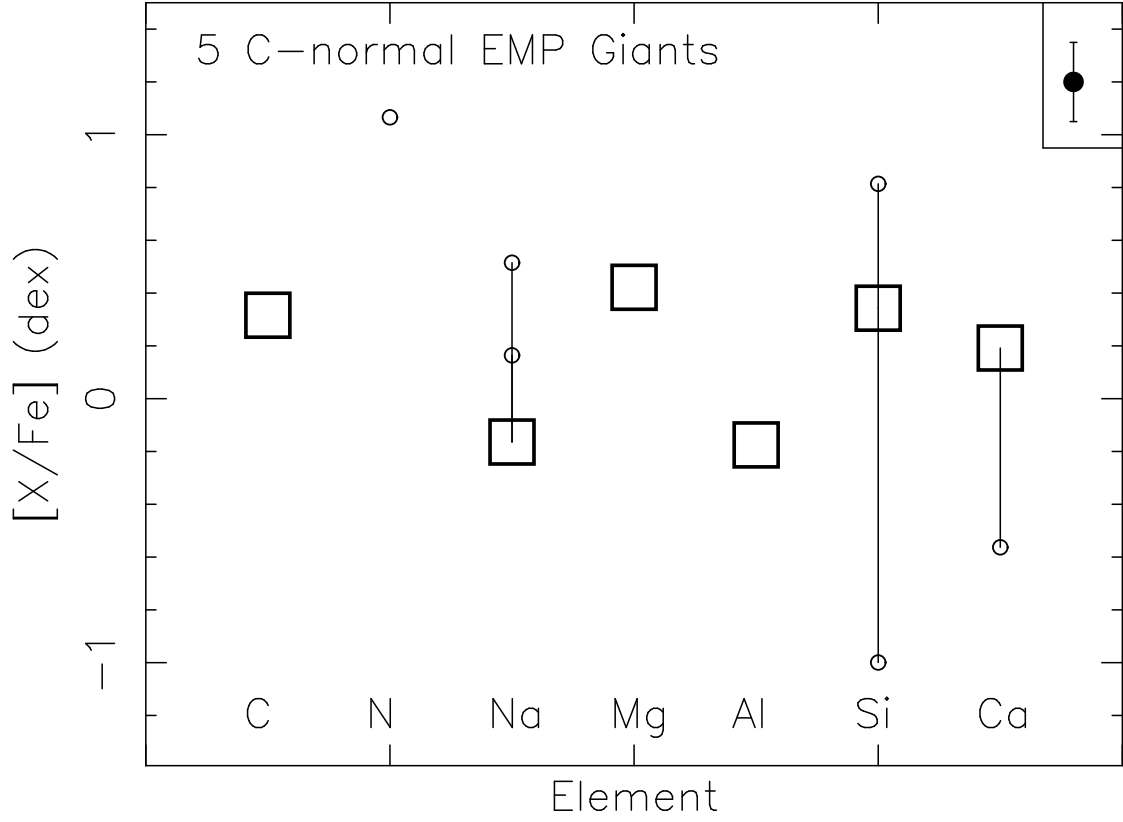


Fig. 6.— The median of $[X/Fe]$ for 7 elements from C to Ca is shown for the 5 C-normal stars as a box. Any ratio $[X/Fe]$ which differs from the median by more than 0.3 dex is shown as a small open circle. Upper limits are excluded. Only one of these stars has a detectable NH band. A typical error bar for each ratio $[X/Fe]$ in a star is shown at the upper right.

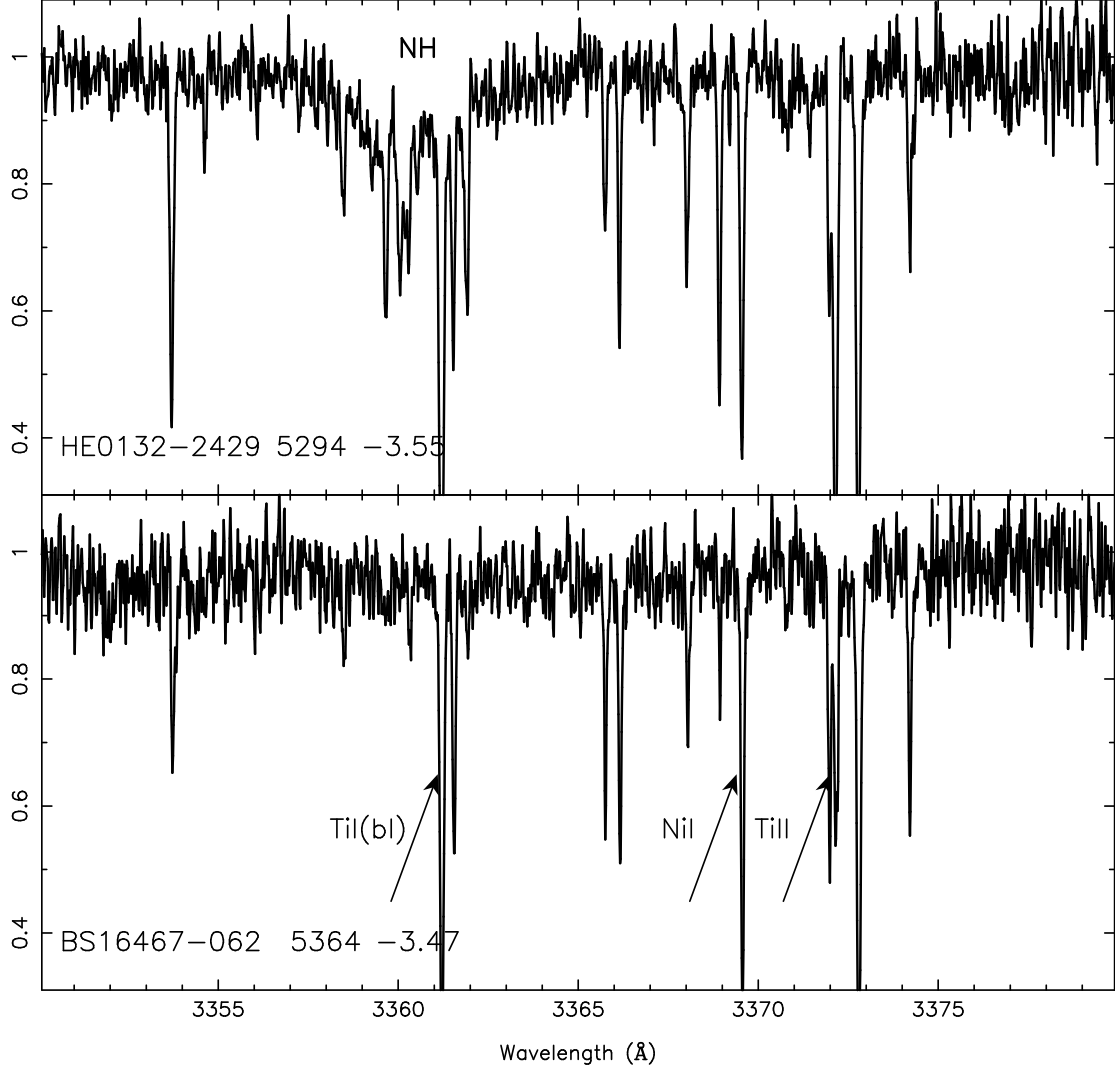


Fig. 7.— The region of the NH band at 3360 Å is shown for two C-normal stars; there is a huge difference in their N abundances. The T_{eff} and $[\text{Fe}/\text{H}]$ for each star are given following the object name in the text within each panel, and the X axis displays rest frame wavelengths in this figure as well as in the next 4 figures.

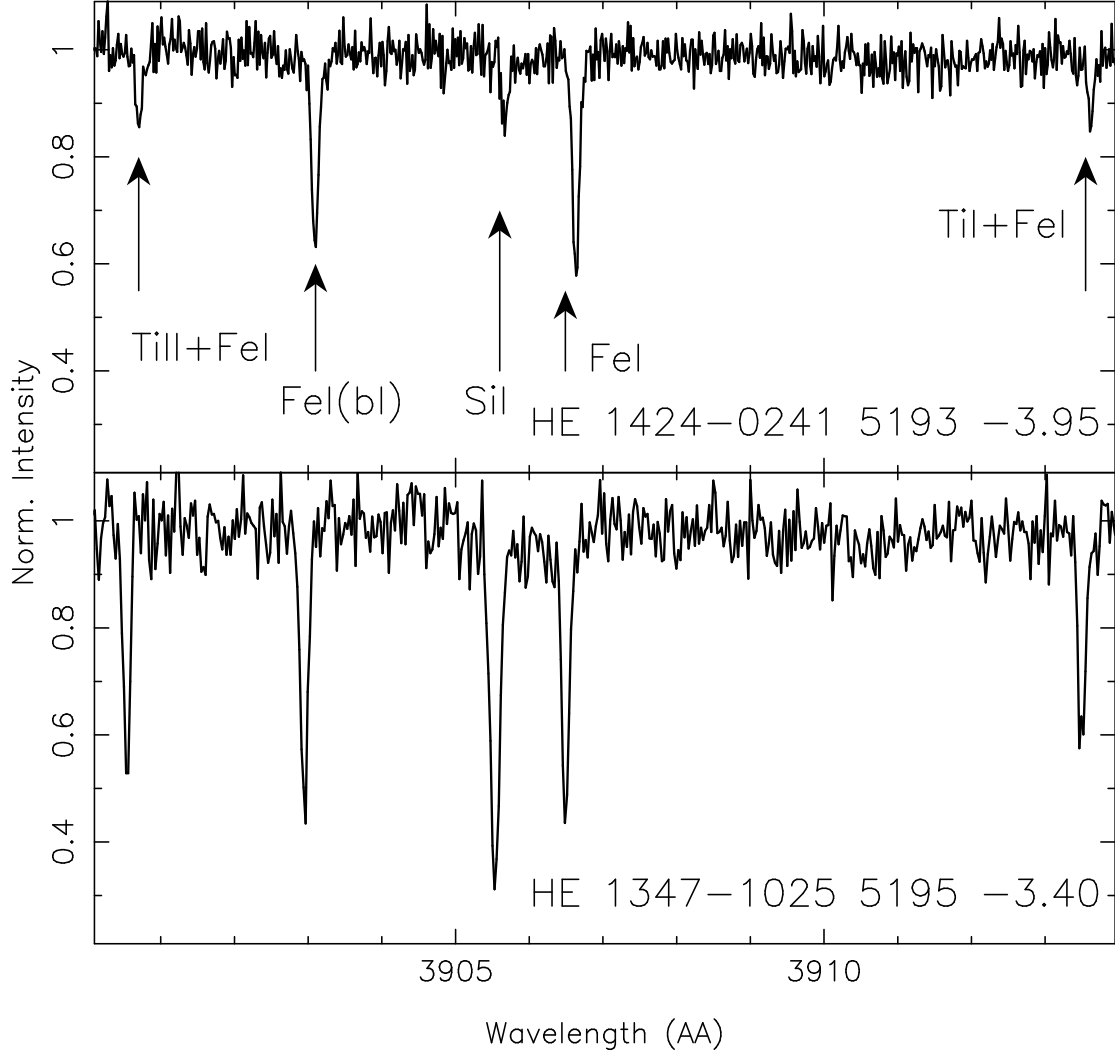


Fig. 8.— The region of the Si I line at 3905 Å is shown in HE 1424–0241 and in HE 1347–1025; the T_{eff} of both stars is the same. Although the Fe-abundance is roughly 4 times higher in the latter star, the ratio of line strengths clearly demonstrates that [Si/Fe] is abnormally low in the former star.

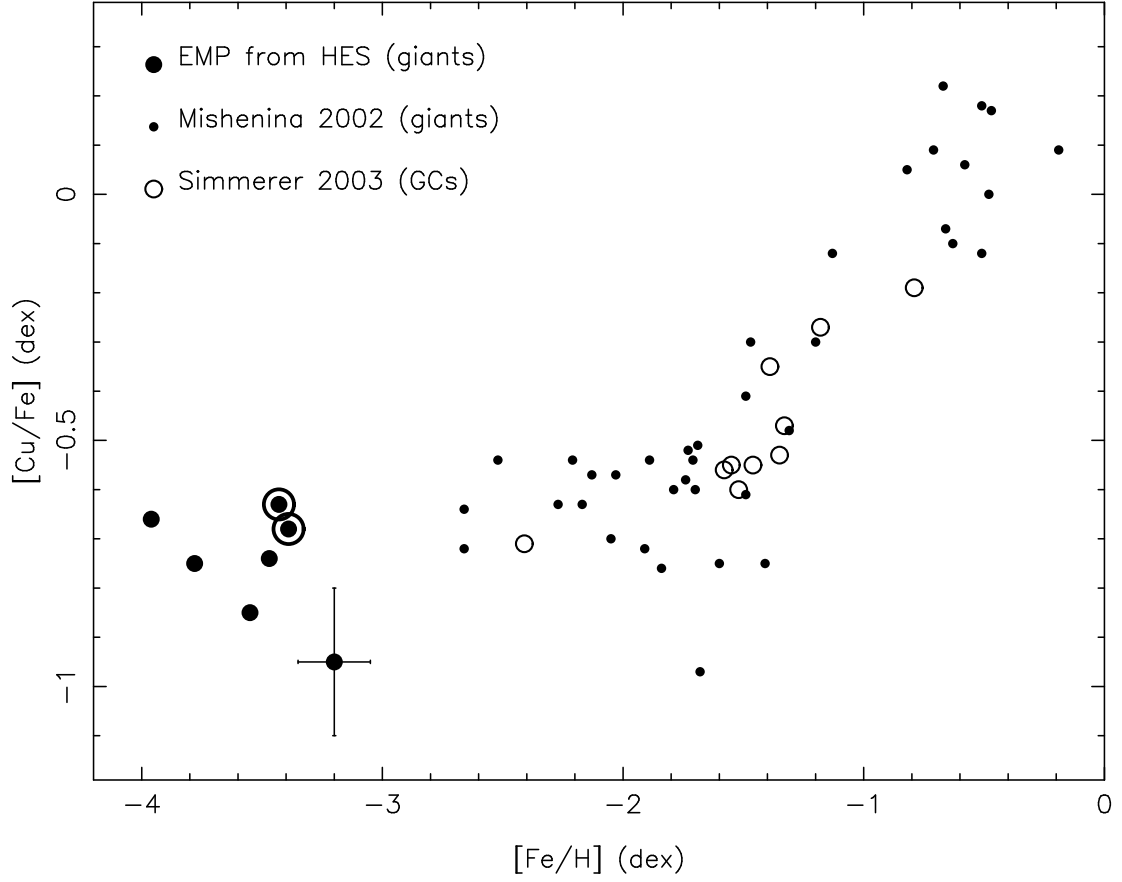


Fig. 9.— $[\text{Cu}/\text{Fe}]$ is shown as a function of $[\text{Fe}/\text{H}]$ for giants, combining data for the extreme EMP stars presented here with that of Mishenina *et al.* (2002) and Simmerer *et al.* (2003). The C-rich stars from the HES are circled.

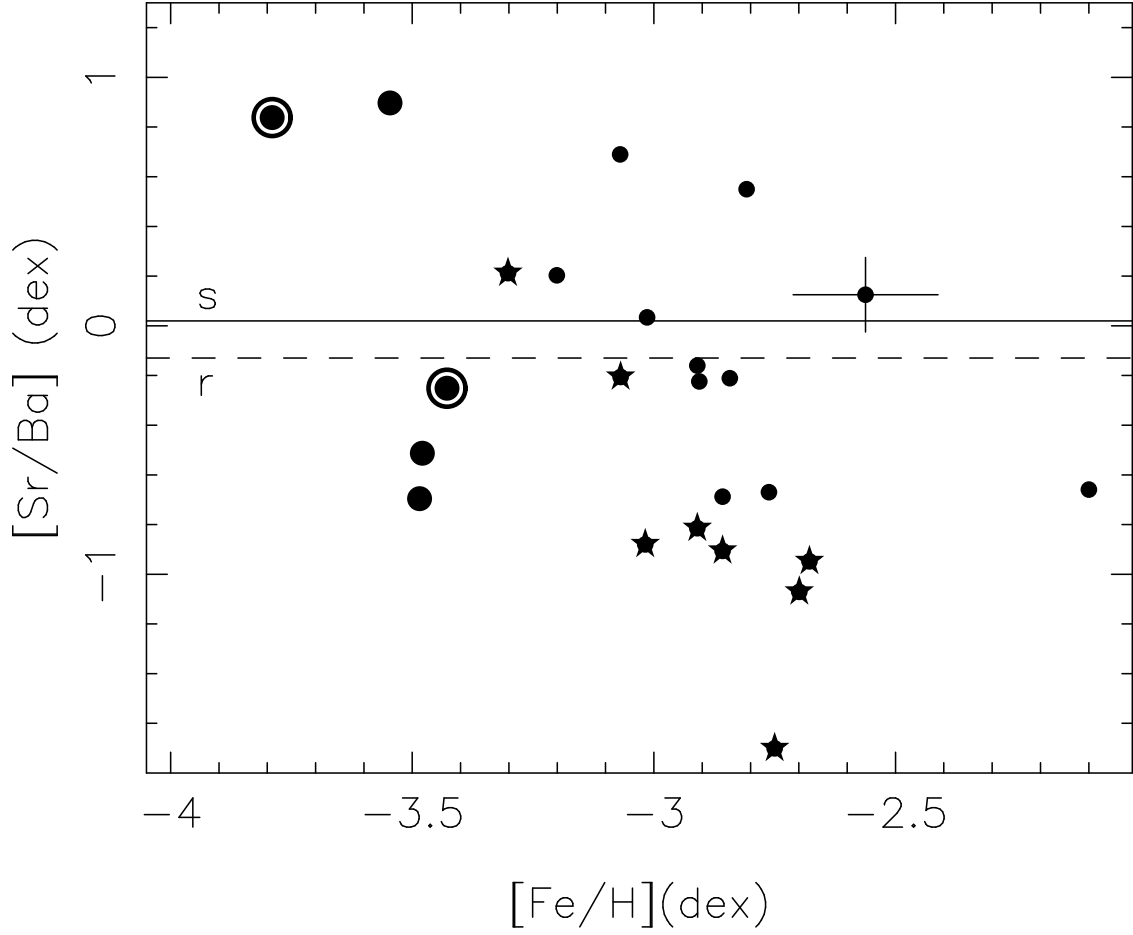


Fig. 10.— $[\text{Sr}/\text{Ba}]$ from singly ionized lines of both elements is shown as a function of $[\text{Fe}/\text{H}]$ for the entire sample of stars from the HES with $T_{\text{eff}} < 6000$ K. Only stars with a secure detection of an absorption feature of at least one of these two species are shown. The stars denote carbon stars with detected bands of C_2 . The large filled circles are the EMP giants in the present sample; those with apparent C-enhancements are circled. A typical error bar is shown for a single star.

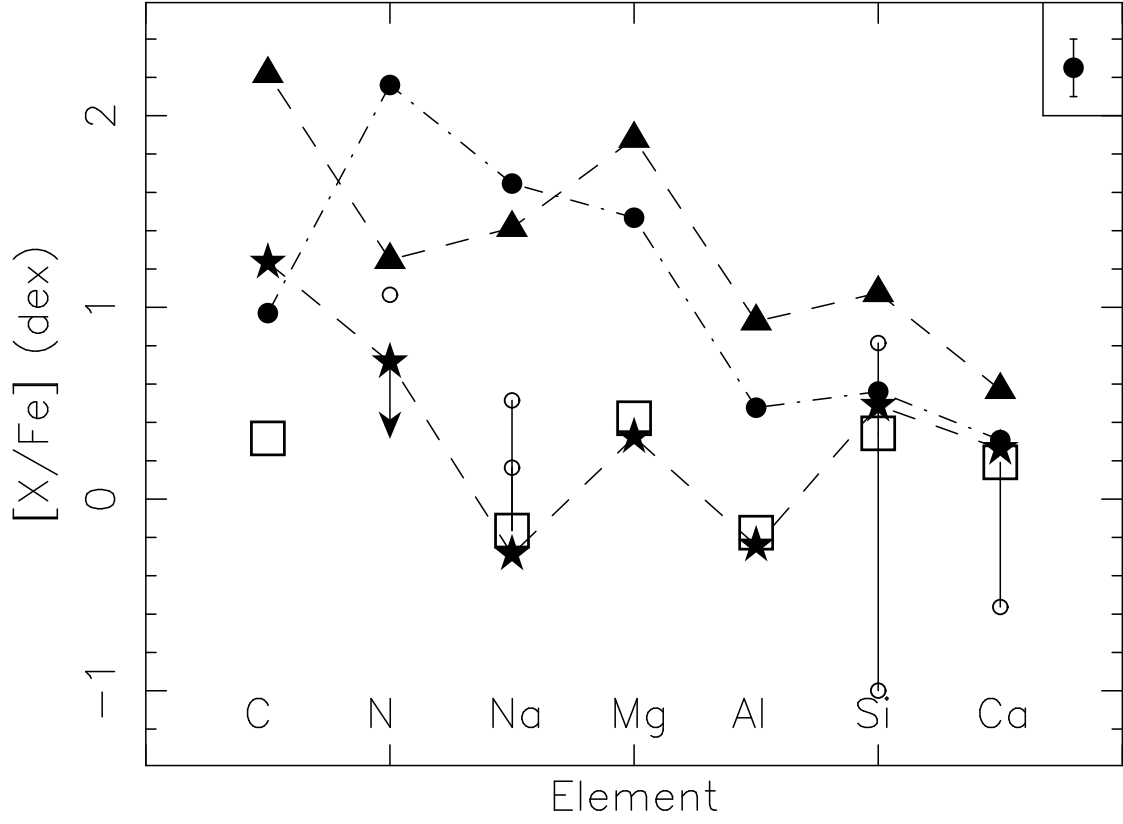


Fig. 11.— The same as Fig. 6. with $[X/Fe]$ for each of the three C-enhanced stars shown as well, indicated by filled symbols. The abundance ratios for each of the C-rich stars are connected by dashed or dot-dashed lines. Upper limits are excluded for the C-normal stars; the single upper limit (for N) which occurs in one C-rich star is indicated. A typical error bar for each ratio $[X/Fe]$ in a star is shown at the upper right.

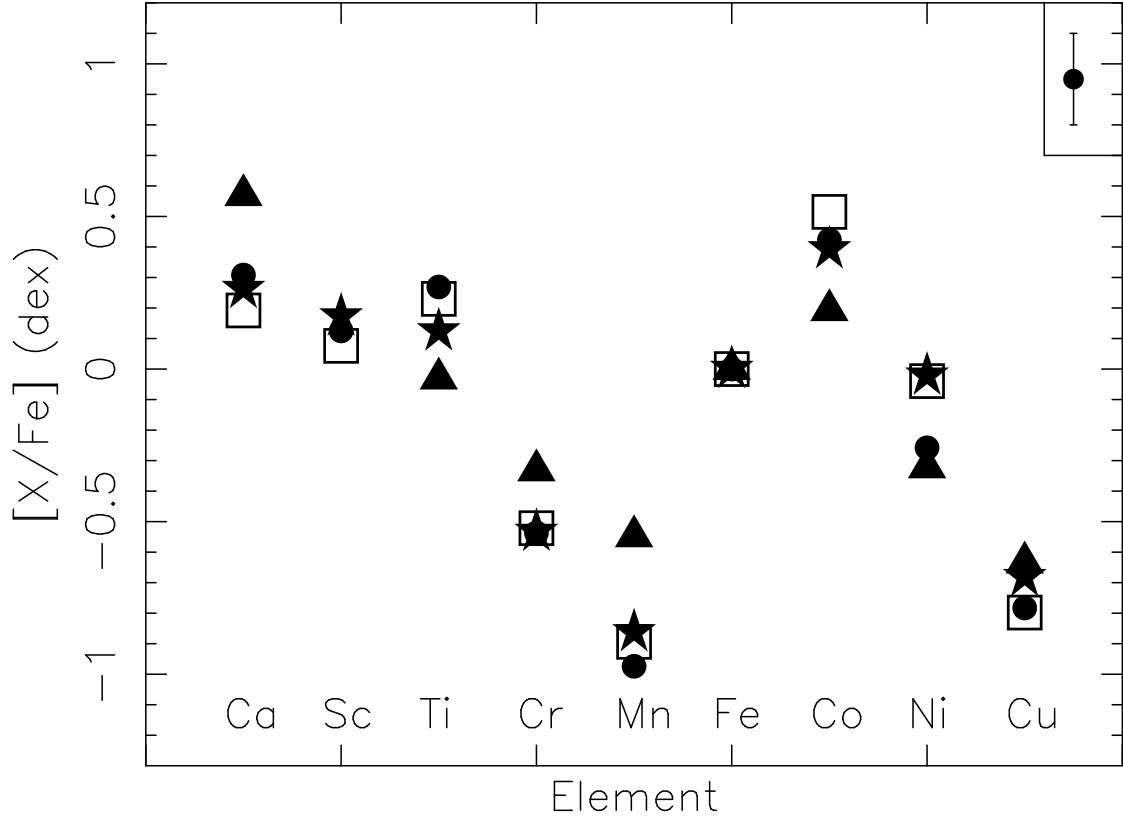


Fig. 12.— $[X/Fe]$ is shown for each of the three C-enhanced EMP stars for 9 elements from Ca to Cu. The median for the five C-normal stars is indicated by a box. A typical error bar for each ratio $[X/Fe]$ in a star is shown at the upper right.

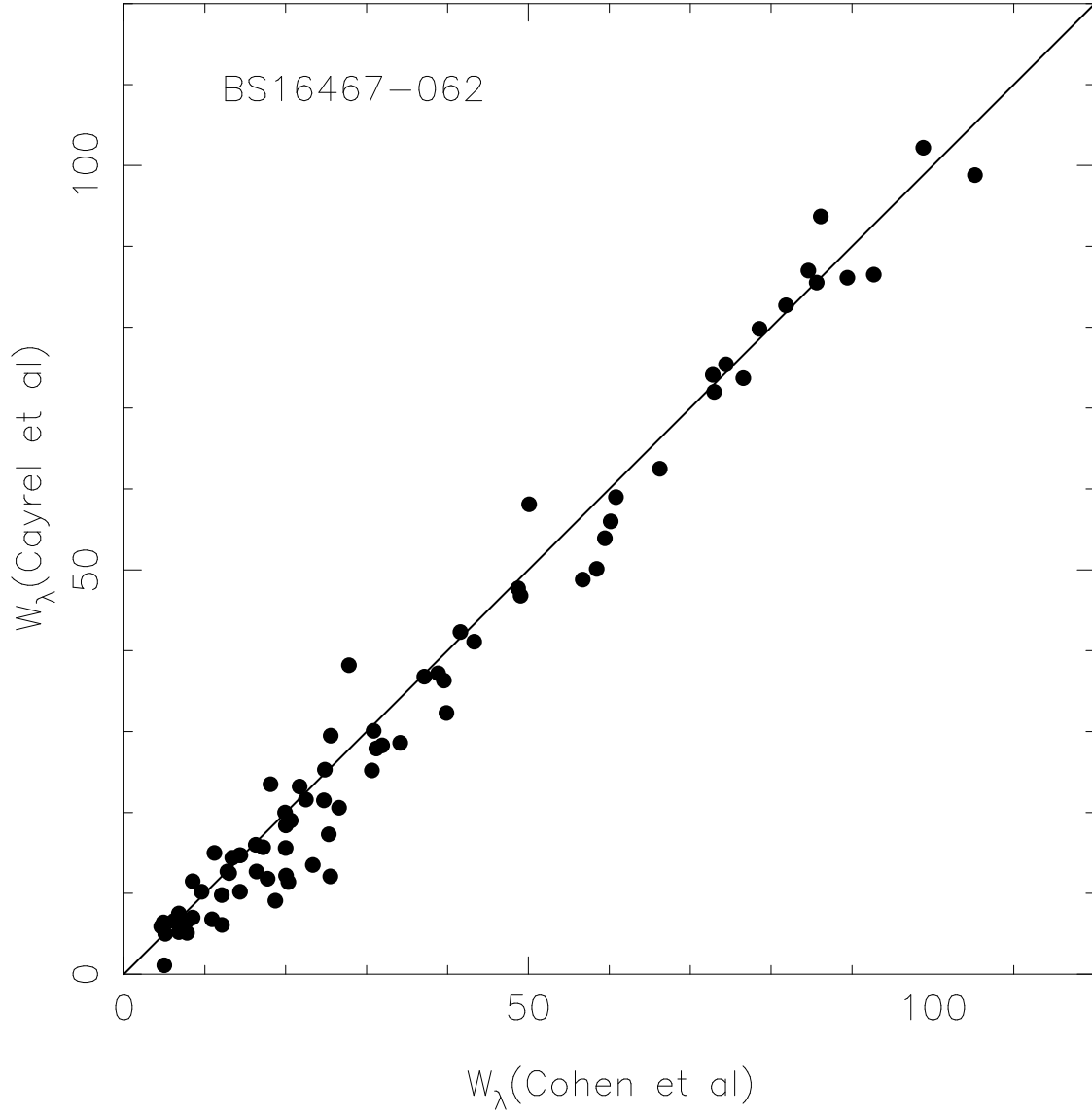


Fig. 13.— The W_λ we measure from our Keck/HIRES spectra for the EMP star BS16467–062 are compared to those of the First Stars VLT/UVES program data from Cayrel *et al.* (2004).

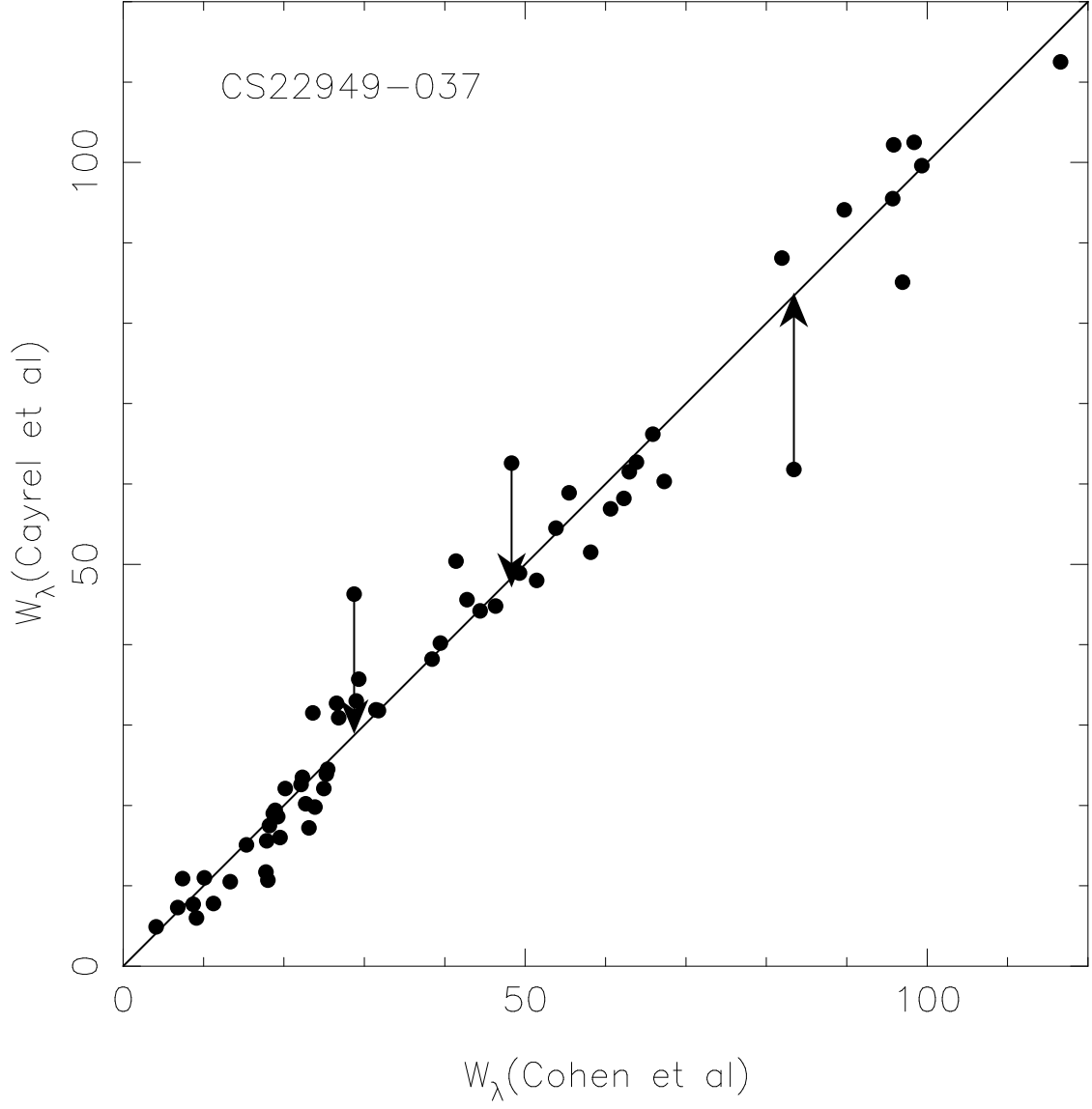


Fig. 14.— The same as Fig. 13 for the star HE2323-0256 (a.k.a. CS22949-037). The arrows denote corrections to the published W_λ of Cayrel *et al.* (2004) (M. Spite, private communication, June 2007).

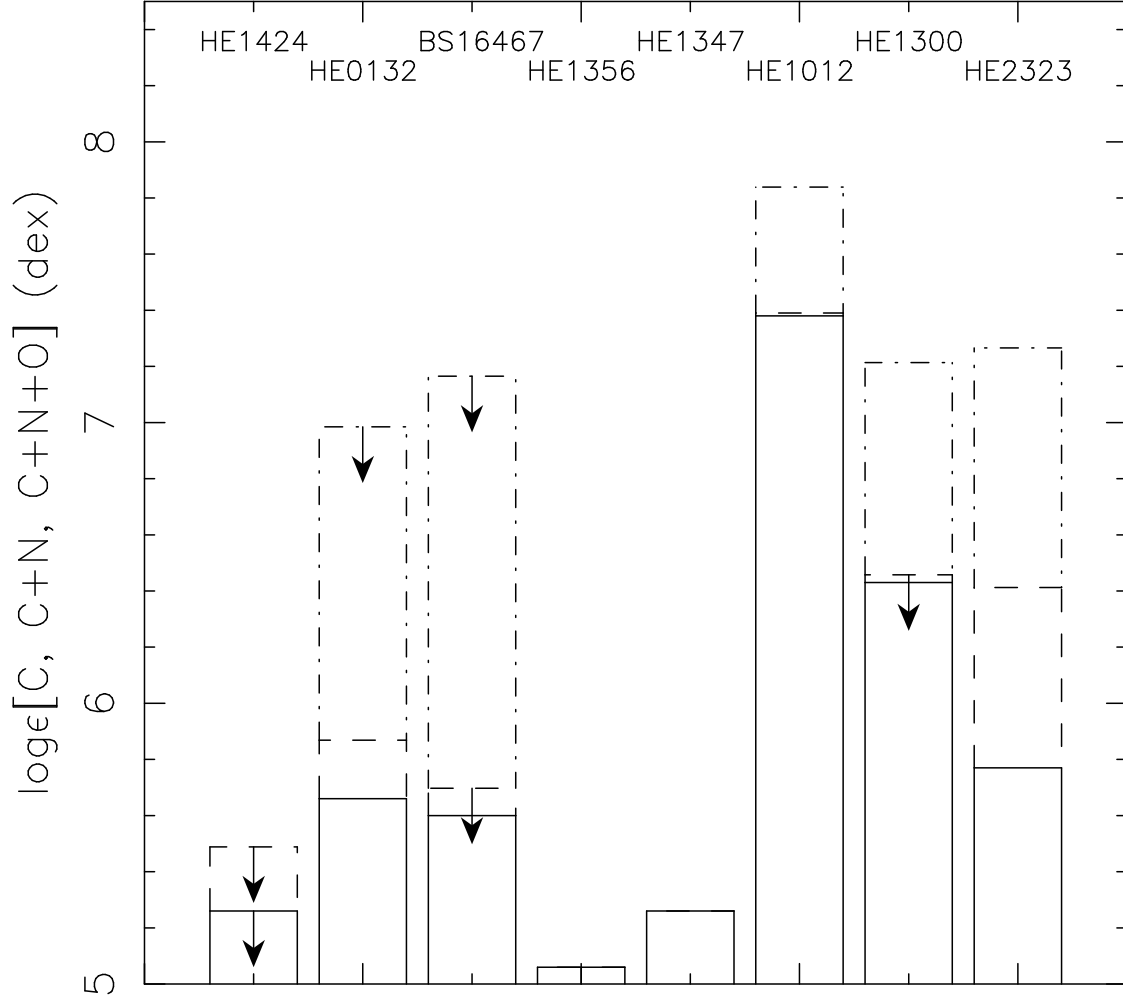


Fig. 15.— $\text{Log} \epsilon(\text{C, C+N, C+N+O})$ is shown for each of the EMP stars in the present sample. The solid horizontal line denotes $\log \epsilon(\text{C})$, the dashed line is $\log \epsilon(\text{C+N})$, while the dot-dashed line shows $\log \epsilon(\text{C+N+O})$. Upper limits are indicated in each case. The 5 C-normal stars are at the left, the 3 higher C stars are at the right side of the plot.

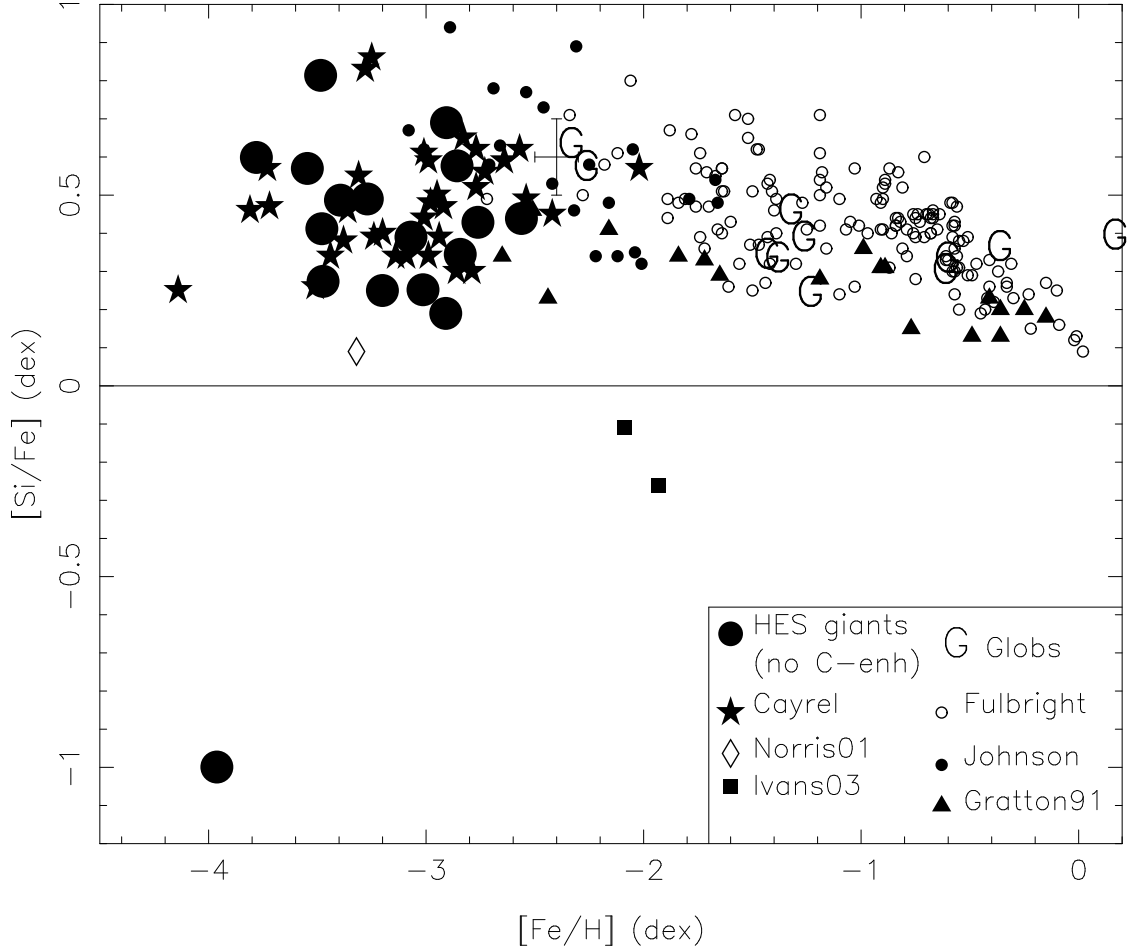


Fig. 16.— $[\text{Si}/\text{Fe}]$ is shown for all of the candidate EMP stars with HIRES spectra analyzed by the 0Z project to date, including the present sample. C-rich stars are not shown. The solid horizontal line denotes the Solar ratio. The plot includes well studied Galactic globular clusters, mostly from analyses by J. Cohen and her collaborators, as well as samples of halo field stars from the sources indicated on the symbol key in the lower right of the figure. Note the highly anomalous position of HE1424–0241, the only star with $[\text{Si}/\text{Fe}] \ll 0$ dex.

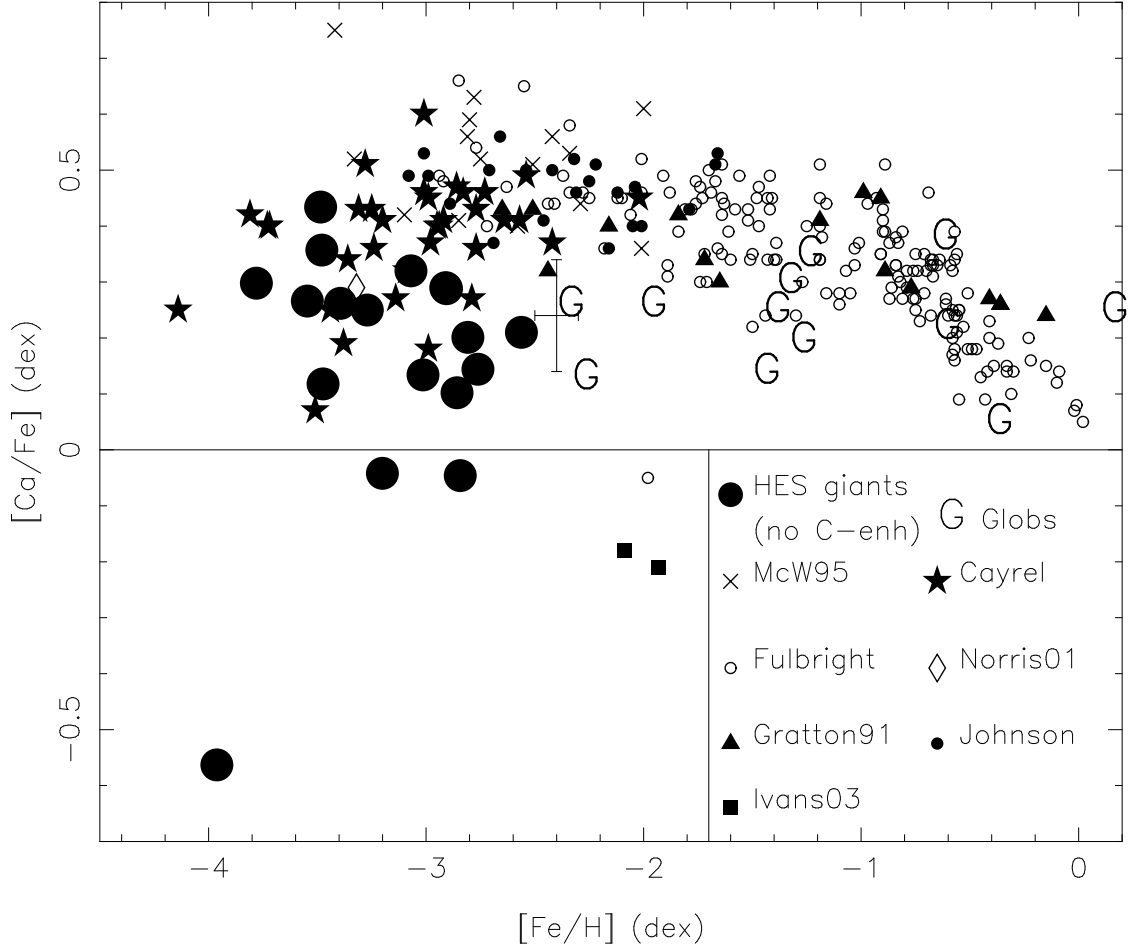


Fig. 17.— $[\text{Ca}/\text{Fe}]$ is shown for all of the candidate EMP stars with HIRES spectra analyzed by the 0Z project to date, including the present sample. C-rich stars are not shown. The solid horizontal line denotes the Solar ratio. The plot includes well studied Galactic globular clusters, mostly from analyses by J. Cohen and her collaborators, as well as samples of halo field stars from the sources indicated on the symbol key in the lower right of the figure. side of the plot. Note the highly anomalous position of HE1424-0241, the star with the smallest $[\text{Ca}/\text{Fe}]$.

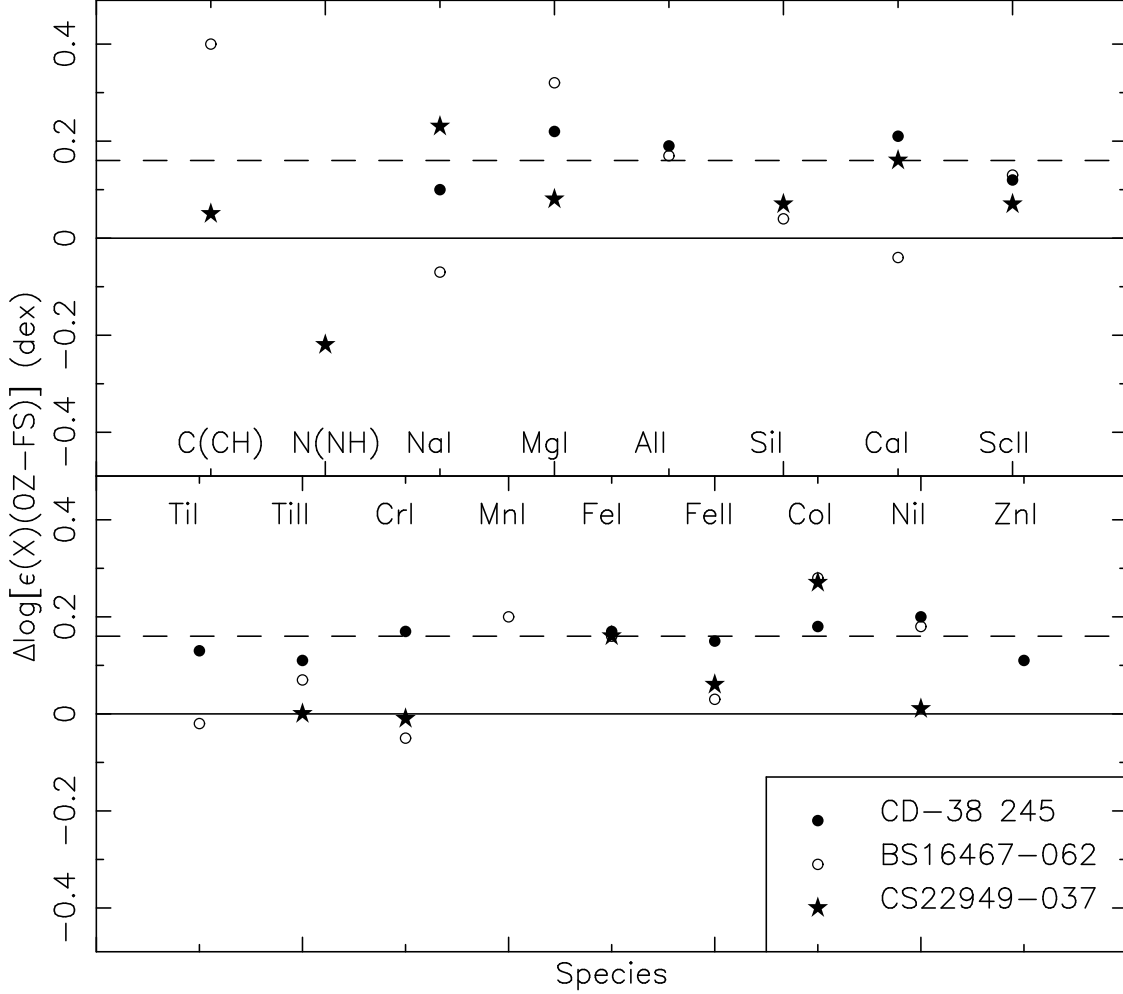


Fig. 18.— The difference for $\log[\epsilon(X)]$ between the our results and those of the First Stars project (Cayrel *et al.* 2004) for three stars. We adopt the stellar parameters used by Cayrel *et al.* (2004) but use our own gf values and set of W_λ , except for CD-38 245, for which we have no HIRES spectra, and for which we adopt those from the First Stars project. The dashed line represents the mean difference for Fe I for the three stars.